Optimal Locations of Sensors and Actuators for Control of a Pedestrian Bridge

by

Fei Liu

A thesis
presented to the University of Waterloo
in fulfillment of the
thesis requirement for the degree of
Master of Mathematics
in
Applied Mathematics

Waterloo, Ontario, Canada, 2021

Author's Declaration

I hereby declare that I am the sole author of this thesis. This is a true copy of the thesis, including any required final revisions, as accepted by my examiners.

I understand that my thesis may be made electronically available to the public.

Abstract

Lightweight structures have been increasing in popularity in structural designs. However, they are more prone to disturbances. Therefore, a controller device can be placed on the structure to control the excessive vibrations. Past works have revealed that there exist corresponding optimal locations on the structure for placing the crucial parts of the controller device, the sensor and the actuator, that result in optimal performance of the controller. The physically practical collocated sensor/actuator design controller device can be moved around and deployed to different structures. The ideally more optimal non-collocated sensor/actuator design allows the sensor and the actuator to be placed separately in their corresponding optimal locations, but it may be physically impractical to implement. Hence, this motivates the study of the optimal locations, and to compare the performances of the non-collocated and the collocated sensor/actuator designs for a lightweight aluminum pedestrian bridge subject to pedestrian walking disturbances. The structure is modelled using the Euler-Bernoulli beam theory, and modal and Hermite basis finite element approximations are applied. The linear-quadratic performance objective control (LQ control) is reviewed and applied. Since approximations are applied, a mapping for the state energy weight in the LQ control performance objective functional from the original functional space to a generic approximation functional space is presented in this thesis.

In the preliminary problem in this thesis, influences of the state weights and the disturbances' spatial distributions on the non-collocated and the collocated sensor/actuator designed linear-quadratic Gaussian (LQG) controllers' optimal locations and comparisons of the performances at their optimal locations are studied on a simplified system model with a Gaussian temporally distributed disturbance. Numerical implementation of disturbances is presented, and numerical complications are discussed and provided with solutions.

The comparisons of the non-collocated and collocated sensor/actuator designs for a more realistic bridge model are made using three different state weights. The realistic bridge model is approximated using the Hermite basis finite element approximation. The $\mathbb{H}_2$-controller is reviewed and applied. The actuator device dynamics and its noise, a reliable pedestrian loading, and a low pass filter are included in this model to consider more realistic disturbances. The results suggest that the physically more practical collocated sensor/actuator design can achieve similar performances as the ideally more optimal non-collocated sensor/actuator design at their corresponding optimal locations.

Acknowledgements

First, I thank my supervisor, Dr. Kirsten Morris, for her patience and expertise in guiding me throughout this research and inspiring me on my academic research path. I like to thank her for training me on finding mistakes as a detective investigating a case, and I learn to face challenges with curiosities instead of fear. English is not my native language, and I used to be intimidated by English writing. However, Dr. Morris' tireless teaching on writing mathematics as a storybook makes me delight in the experience of writing my thesis.

I like to thank my co-supervisor, Dr. Sriram Narasimhan, for his guidance in the engineering field and his teaching, especially for his patience and clarity in explaining the field specialized materials to me to make this thesis cross-disciplinary.

I also like to thank Dr. Henry Shum for being the chair of my thesis presentation and Dr. Jun Liu and Dr. Naveen Chandrashekar for serving on my committee and providing valuable comments and insights. Moreover, I would like to thank Dr. Jun Liu for teaching me the first course on Control Theory.

There are many other people that I would like to thank for where I am today. But in this limited space, I will dedicate my gratitude to those who are relevant in the University of Waterloo. I like to thank Ala and Brian from my research group for acting like an older sister and younger brother to support me outside of academic settings.

For the most, I sincerely thank my parents for supporting me with love and cares. I deeply thank my mother, who took care of me during the entire pandemic work from the home period. For me, she is like an optimal estimator that estimates my true emotional state and an optimal control that always provides me with unconditional love as feedback, to heal me from all the pressures and downs in life. I love you.

Table of Contents

List of Figures

List of Tables

Chapter 1

Introduction

Figure 1.1: Photo of an aluminum pedestrian bridge from [13].

Lightweight structures, such as an aluminum pedestrian bridge shown in Figure 1.1, have been increasing in popularity in structural designs. However, due to their compositions of lightweight materials, they are more prone to disturbances that will cause vibrations that could lead to serviceability and safety issues. A device can be placed on the structure to control the excessive vibrations. Past works have revealed that there exist optimal locations on the structure for placing parts of the controller device, the sensor and the

actuator, that result in optimal performance of the controller. Physically, the sensor and actuator can be designed on a single device, and be placed at the same location with respect to the structure. This is known as collocated sensor/actuator design. Figure 1.2 shows a collocated sensor/actuator design controller: the deployable control system prototype controller that has been studied in the work [16]. This compact controller device can move around and deploy to different structures, and it is physically practical. On the other hand, the sensor and the actuator can be placed at their corresponding optimal locations, and not constrained to a single location as in the collocated sensor/actuator design. This is known as non-collocated sensor/actuator design, and ideally, this should yield a better controller performance. However, in reality, it is physically impractical to implement on structures, and it often causes serious time delay issues. Hence, one may wish to use the more physically practical collocated sensor/actuator design while aiming for the ideally more optimal non-collocated sensor/actuator design's performances. Thus, the challenge of the significance of the difference in their performances is addressed in this thesis.

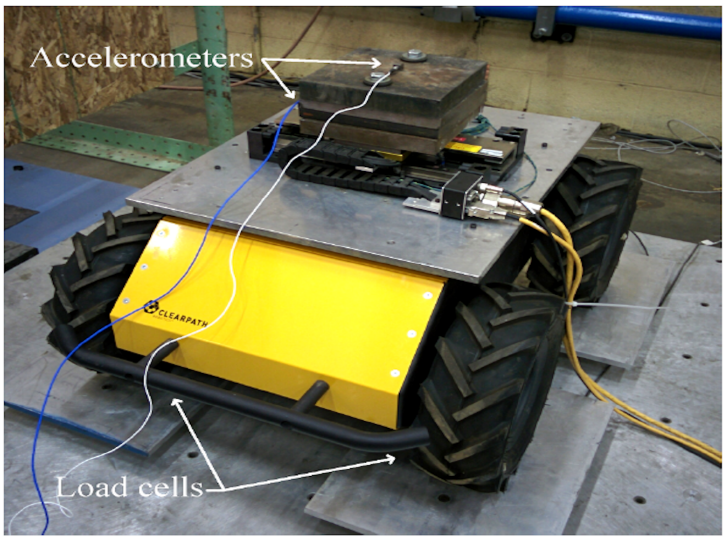

Figure 1.2: Photo of a controller device, the deployable control system prototype controller from [16].

In this thesis, the non-collocated sensor/actuator and the collocated sensor/actuator optimal controllers are designed for a lightweight aluminum pedestrian bridge. The main goal of this thesis is to study and compare their performances as a function of their loca-

tions on the bridge subject to pedestrian walking loads.

The control studies conducted on the bridge structure system in this thesis are carried out using mathematical models to approximate and simulate the vertical direction responses of the bridge structure system subject to disturbances. The controllers are designed, and the resulting algorithms are applied to the mathematical models in simulations.

The controller's algorithm to be designed in this thesis consists of an estimator that estimates the states and a control law that uses the estimation of the states to stabilize the system. The optimal estimator achieves minimal estimation error and the optimal control law achieves a balance between the control effort spent and the system's total energy. The combination of the optimal estimator and optimal control yields an optimal controller.

The controller device that executes the control algorithm consists of two crucial physical components, a sensor and an actuator, that work together to effectively control the system. The sensor measures the vibration signals at its location that are fed into the estimator for estimating the state of the system. The actuator receives information from the control law and applies control forces at its location to stabilize the system.

Structural vibrations are a combination of different sinusoidal signals with corresponding nodes and anti-nodes. To suppress vibrations, applying a control force at the anti-node location is the most effective. Therefore, certain locations along a long flexible structure are more easy to control than other locations. Similarly, to estimate an accurate system subjected to disturbances, measurements at certain locations are more helpful. Hence, the placement of the controller crucially influences the controller's performance, and the controller should be placed at the optimal location. Consequently, the optimal non-collocated sensor/actuator design and the optimal collocated sensor/actuator design may yield different controller's performances at their optimal locations. Since the non-collocated sensor and actuator can be at their corresponding optimal locations without being constrained to a single location as in the collocated sensor/actuator design, the non-collocated sensor/actuator design yields a better controller performance ideally. However, as mentioned above, the non-collocated sensor/actuator design is physically impractical compare to the collocated sensor/actuator design.

A preliminary problem of a simplified model, a modal approximated unit parameter beam, is first simulated in Matlab. Implementation and the associated numerical issues

are discussed. Results are presented to study various parameters' influence on the optimal controlled response and the optimal locations of the non-collocated and collocated sensor/actuator designs. Then, a more realistic model of a lightweight aluminum pedestrian bridge is set up for disturbance control. Since the controller is a physical device that is being attached to the bridge, the interaction between the structure and the controller must be considered. In this thesis, the sensor is assumed to be relatively lightweight and its mass can be neglected. The actuator device is assumed to weigh 2% of the bridge mass. Thus, the actuator dynamics are modelled as a coupled spring-mass-damper (SMD) system to the bridge.

The bridge controller aims to reduce the vibrations along the entire bridge (state response) subject to all frequencies in the domain of a predictable pedestrian walking disturbance, while achieving a balance between the control effort and the bridge's transient and equilibrium states so that a pedestrian perceives it as a stable bridge (comfort level for the pedestrian). Since the pedestrian walking frequencies are in the lower frequency ranges ($< 3Hz$) as shown in [13], a low pass filter that targets the rejections in the lower frequency disturbance response is applied. Since the pedestrian walking disturbance is known, the disturbance is modelled as a coupled dynamical system to the bridge. An actuator device noise is included in the model, and this results in the estimator design's dependency on both the actuator and sensor locations.

Numerical simulations on the bridge-pedestrian model using the optimal non-collocated sensor/actuator and the optimal collocated sensor/actuator controllers are conducted in Matlab. Analysis of the optimal locations and the controlled responses resulting from the two controllers is conducted. The simulation results show that the differences in the two controllers' performances at their optimal locations are not significant, and the collocated sensor/actuator design potentially performs as excellently as the non-collocated sensor/actuator design. The results suggest that the physically more practical collocated sensor/actuator design can achieve similar performances as the ideally more optimal non-collocated sensor/actuator design at their corresponding optimal locations.

1.1 Literature Review

There are many closed loop feedback control designs that can achieve different control objectives. Feedback control using state information to stabilize the system via a gain of

the state while minimizing a performance index/control objective (usually an indication of some type of energy spend on stabilizing the system) is called an optimal closed-loop controller. The works in [44] and [45] compared three control laws for non-stochastic (constant pulse load disturbance) systems: direct proportional feedback, constant-gain negative velocity feedback and the optimal linear-quadratic regulator (LQR), and revealed that the LQR optimal control achieved a better balance between control effort and system responses while associated with a lower peak actuator forces. The optimal LQR achieves system stabilization with minimal linear-quadratic (LQ) performance index, known as the LQ performance index. The LQ performance index is in the form of a linear combination of the weighted total system state and the control spent for stabilization.

Often, only partial state information is obtained, and an estimator is required to construct the full state feedback. This is called the output feedback controller design. The optimal estimator achieves full state estimation with minimal performance index, such as the LQ performance index in the form of the estimation error variance.

Different designs of optimal output feedback controllers are designed for different control goals. The linear-quadratic Gaussian (LQG) controller is used to control random initial condition response and Gaussian disturbance response of a stochastic system, which is the combination of the optimal LQ control and the optimal LQ estimator (or the Kalman Filter if the covariances of the noises are known). The $\mathbb{H}_2$ controller is used to control a known non-Gaussian disturbance. It is also based on the LQ controller performance index, but with the disturbance being modelled as part of the system as demonstrated in [33]. The $\mathbb{H}_\infty$ controller is used to control an unknown or a spatio-temporally varying disturbance as shown in [11].

Previous works have shown that the locations of the sensor/actuator placements impact the performance of the control and estimation aspects significantly, and the optimal locations of the sensor/actuator have been studied. There are many objective functionals that can be considered for finding the controller's optimal locations. The two main approaches are: 1. Using the controller design performance index as the cost functional, and 2. Combining multiple objectives. The controller design performance index, parameterized with sensor/actuator location(s) can be used as the cost functional for finding the optimal locations of the sensor/actuator. Reviews and comparisons on the methods for finding the optimal sensor/actuator locations can be found in [36] and in [18]. They revealed that LQ performance criterion should be preferred over controllability criterion. Although the controllability (observability) criterion can be used for choosing the sensor/actuator can-

didate locations, it is shown that this type of location optimization is mode dependent, and the optimal location becomes non-optimal when the approximation on the number of modes (or number of finite elements) increases [36]. Thus, further discussions on the controllability and/or observability criterion will not be included, and readers may refer to the works in [19], [49], [27] and [47] for sensor/actuator location optimization based on the controllability and/or observability criterion.

Theories on the existence of optimal location(s) of the Kalman estimator's sensor(s) and the optimal LQ control's actuator(s) can be found in the works [34] and [50]. For non-disturbance (or non-stochastic disturbance) systems, the works [10] and [14] studied separately locating the sensor and actuator using the LQ performance index and [45] studied the collocated sensor/actuator case. They revealed that placing the sensor and actuator at their optimal locations resulted in a faster decay of the state response, smaller energy norm, and faster decay in input control. For a Gaussian disturbance system, the work [23] proved the existence of the optimal sensor/actuator location pairs of the collocated and non-collocated LQG controllers. The optimal locations of the non-collocated sensor/actuator was compared with those of the collocated sensor/actuator. This work also revealed that separately computing optimal locations for the sensor and actuator were computational advantageous but yielded a higher optimal performance index value.

For known distributed disturbance systems, the works [35],[30] and [29] used the $\mathbb{H}_2$ criterion to find the optimal non-collocated and/or collocated sensor/actuator locations. These works revealed that disturbance and sensor locations influenced the optimal placement of the actuator, and the non-collocated optimally located sensor/actuator pair could improve the performance of the closed-loop system by $40\% - 50\%$ in terms of the spatial $\mathbb{H}_2$ norm.

For spatial-temporal varying or unknown parameter distributed disturbance systems, the work [26] established the conditions for well-posedness of the approximation $\mathbb{H}_\infty$ actuator optimization problem and [26] developed a non-gradient based location optimization approach.

Besides using the location parameterized controller design performance index for selecting the optimal locations for a distributed parameter system, structural control works in [42], [20], and [52] used other location optimization criteria to find the optimal location, and then applied LQG control at the fixed optimal location. The work [37] developed an iterative optimal location finding method, with $\mathbb{H}_2$ criterion for optimal sensor location and $\mathbb{H}_\infty$ criterion for optimal actuator location, and showed that this method were performed

in the aforementioned paper requires much less computation time compared to iterative method.

The work [11] studied a switching scheme for multiple collocated sensor/actuator pairs placed at optimal locations with multiple optimization criteria. However, the switching sensor/actuator could only do better than a single fixed actuator but no better than a fixed two-actuator configuration. Extended work can be found in [12].

The weightings in the LQ performance index impact the effectiveness of the controller significantly. Studies on the selection of the weighting matrices in the LQ performance index for controlling beam structures can be found in [20], [4], [22] and [1]. These works revealed that weighting the state proportional to the system's potential and kinetic energy could achieve high damping ratio.

The work [5] revealed that the interaction between the structure and a mass (human) may affect the vibration dynamics significantly and should be considered as a coupled dynamical system to the structure. The work [24] considered the interaction between a attached mass (sensor) and the structure as a coupled dynamical system, which was derived from the Hamilton's Principle.

The performance comparison between the collocated and non-collocated sensor/actuator designs for lightweight pedestrian bridges has not been involved in the current literature. The work [16] has shown that the collocated sensor/actuator deployable prototype controller device is economical for short term control applications on lightweight structures. However, there is no comparisons done between the physically practical collocated sensor/actuator design and the ideally more optimal non-collocated sensor/actuator design. The main goal of this thesis is to study the differences in the optimally located non-collocated sensor/actuator and collocated sensor/actuator controllers' performances.

Chapter 2

System Model

The physical system in this research consists of a lightweight aluminum pedestrian bridge, a sensor device, an actuator device, and walking pedestrians. The bridge is considered as the plant being controlled. The sensor device provides measurements to the controller, and the actuator device applies the control forces to the plant based on the control algorithm. The pedestrian load is considered as an external disturbance to the plant.

2.1 Plant Model

Pedestrians exert disturbance forces in both the vertical and horizontal directions, but only vibrations in the vertical direction are studied in this thesis. The control on the vertical displacement and velocity response of the bridge is considered in this research.

The plant model is based on the Euler-Bernoulli beam theory in one-dimensional space. The key assumptions in the Euler-Bernoulli beam theory are:

- the normals to the midline always remain straight and normal, and
- the midline deformation angle θ is small.

Denote the bridge's deflection as $w(x,t)$, the bending moment as $m(x,t)$, the control force as $b_r(x)u(t)$ and the pedestrian disturbance as $g_p(x)\omega_p(t)$. The dynamics of the bridge

are modelled by the initial boundary value problem (IBVP)

$$\rho\frac{\partial^2 w(x,t)}{\partial t^2} + c_d\frac{\partial w(x,t)}{\partial t} + \frac{\partial m^2(x,t)}{\partial x^2} = b_r(x)u(t) + g_p(x)\omega_p(t), \tag{2.1.1}$$

$$\begin{aligned} w(0,t) &= 0 = w(L,t), \\ m(0,t) &= 0 = m(L,t). \end{aligned} \tag{2.1.2}$$

$$\begin{aligned} w(x,0) &= w_0(x), \\ \frac{\partial w(x,0)}{\partial t} &= v_0(x), \end{aligned} \tag{2.1.3}$$

where ρ is the density parameter and c_d is the vicious damping parameter.

The term $m(x,t)$ can be expressed in terms of deflection $w(x,t)$ and velocity $\frac{\partial w(x,t)}{\partial t}$ as

$$m(x,t) = k_d\frac{\partial^3 w(x,t)}{\partial t \partial x^2} + EI\frac{\partial^2 w(x,t)}{\partial x^2}, \tag{2.1.4}$$

where k_d is the Kelvin-Voigt damping parameter, E is the Young's modulus, and I is the moment of inertia parameter.

Expanding the moment term (2.1.4) in (2.1.1), and the following expression is obtained:

$$\rho\frac{\partial^2 w(x,t)}{\partial t^2} + c_d\frac{\partial w(x,t)}{\partial t} + k_d\frac{\partial^5 w(x,t)}{\partial t \partial x^4} + EI\frac{\partial^4 w(x,t)}{\partial x^4} = b_r(x)u(t) + g_p(x)\omega_p(t). \tag{2.1.5}$$

The term $b_r(x)u(t)$ models the control force from the actuator with width Δ, where $b_r(x)$, parameterized with the actuator's center location r, is the spatial distribution of the control force $u(t)$. The actuator location is denoted by

$$b_r(x) = \begin{cases} \frac{1}{\Delta} & , |r-x| < \frac{\Delta}{2} \\ 0 & , |r-x| \geq \frac{\Delta}{2} \end{cases}. \tag{2.1.6}$$

The term $g_p(x)\omega_p(t)$ models the disturbance due to n_p pedestrians, where $g_p(x)$ is the spatial distribution of the pedestrian load, and $\omega_p(t)$ is the temporal walking disturbance. Since controlling the vibrations over the entire bridge is considered, the disturbance is assumed to be uniformly applied to the beam. Thus, $g_p(x) = \frac{n_p}{L}$. The temporal amplitude $\omega_p(t)$ of the input disturbance is the temporal ground reaction force (2.1.7) [13] from the walking of the pedestrian,

$$\omega_p(t) = W_{ped} + W_{ped} \sum_{k=1}^{r_p} \eta_k \sin(2\pi k f_p t + \psi_k), \tag{2.1.7}$$

where W_{ped} is the average weight of the pedestrian, f_p is the pacing frequency in Hz, η_p^k is the periodic load factor (DLF) for the k^{th} harmonic, ψ_k is the phase angle of the kth harmonic, r_p is the total number of harmonics considered.

The pedestrian mass is assumed to be $70kg$. Earth's gravity is assumed to be $9.81m/s^2$. The fundamental mode of the walking load is considered, with pacing frequency $f_p = 1.6Hz$ and DLF $\eta_p^1 = 0.37$ [13]. The temporal pedestrian disturbance is simplified to

$$\omega_p(t) = W_{ped} + W_{ped} 0.37 \sin(3.2\pi t), \tag{2.1.8}$$

where $W_{ped} = 70kg \times 9.81m/s^2$.

In the context of control, systems are usually presented in state-space form. Define the space $\mathcal{H}^2(0,L) = \{\phi \in \mathcal{L}_2(0,L) : \phi' \in \mathcal{L}_2(0,L), \phi'' \in \mathcal{L}_2(0,L)\}$, the space $\mathcal{H}_s(0,L) = \{w \in \mathcal{H}^2(0,L), w(0) = 0, w(L) = 0\}$ and the state-space $\mathcal{Z}_{inf} = \mathcal{H}_s(0,L) \times \mathcal{L}_2(0,L)$. With state $z_b(t) = [w(.,t), v(.,t)]$, $v(.,t) = \frac{\partial w}{\partial t}(.,t)$, the state-space formulation of equation (2.1.5) is

$$\frac{dz_b}{dt}(t) = A_b z_b(t) + B_{1b}\omega_p(t) + B_{2b_r} u(t), \tag{2.1.9}$$

where

$$A_b = \begin{bmatrix} 0 & I \\ -\frac{d^4}{dx^4} & -c_d - k_d \frac{\partial^4}{\partial x^4} \end{bmatrix}, B_{1b} = \begin{bmatrix} 0 \\ g_p(x) \end{bmatrix}, B_{2b_r} = \begin{bmatrix} 0 \\ b_r(x) \end{bmatrix}. \tag{2.1.10}$$

The domain of A_b is

$dom(A_b) = \{(w,v) \in \mathcal{Z}_{inf} : w'' \in \mathcal{H}_s(0,L), v'' \in \mathcal{H}_s(0,L)\}$.

It is known from the textbook [32] that A_b with domain $dom(A_b)$ generates an exponentially stable semigroup on $\mathcal{Z}_{inf}$.

The sensor is located at an interval on the bridge to measure the deflection. Let $y_2(t)$ denote the sensor output,

$$y_2(t) = c_l(x) z_b(x,t), \tag{2.1.11}$$

where $c_l(x)$ denotes the characteristic of the sensor location with its center at $x = l$ and its width is the same as the actuator's,

$$c_l(x) = \begin{cases} \frac{1}{\Delta} & , |l-x| \leq \frac{\Delta}{2} \\ 0 & , |l-x| > \frac{\Delta}{2} \end{cases}. \tag{2.1.12}$$

2.2 Numerical Approximations

Since a closed-form solution to the system (2.1.5) is not available, the Galerkin's approximation method is applied to approximate a system of equations that has closed-form solutions. For any positive integer $n \in \mathbb{Z}_+$, $n = 1, 2, ..., N$, denote the approximation basis as ϕ_n and let $\mathcal{H}_n(0, L)$ be the span of ϕ_n. Let $w^N(x,t) = \sum_{n=1}^{N} w_b^n(t)\phi_n(x)$ be the approximation solution, where w_b^n denotes the time coefficient of the n^{th} basis.

In the preliminary problem, modal approximation is applied. Let w_b^n denote the coefficient of the n^{th} mode, $n = 1, 2, ..., N$. Define $\mathcal{H}_n(0, L) = \mathcal{H}^2(0, L) \cap \mathcal{H}_0^1(0, L)$, where

$\mathcal{H}_0^1(0, L) = \{\phi \in \mathcal{L}_2(0, L) : \phi' \in \mathcal{L}_2(0, L), \phi(0) = \phi(L) = 0\}$.

Choose $\phi_n(x) \in \mathcal{H}_n(0, L)$ to be the eigenfunctions of $\frac{\partial^4 w(x,t)}{\partial x^4}$ with boundary conditions (2.1.2),

$$\phi_n = \sin(\frac{n\pi x}{L}). \tag{2.2.1}$$

Denote the approximated deflection coefficients as $w_b^N \in \mathbb{R}^N$ and the approximated system is a system of second order ODEs

$$M\ddot{w_b^N}(t) + D\dot{w_b^N}(t) + Kw_b^N(t) = B_{r_{pos}}^N u(t) + B_d^N \omega_p(t), \tag{2.2.2}$$

where

M : $N \times N$ diagonal matrix with $M_{n,j} = \int_0^L \rho \phi_n \phi_j dx$,

D : $N \times N$ diagonal matrix with $C_{n,j} = \int_0^L [c_d \phi_n \phi_j dx + k_d \phi_n'' \phi_j'']dx$,

K : $N \times N$ diagonal matrix with $K_{n,j} = \int_0^L EI \phi_n'' \phi_j'' dx$,

$B_{r_{pos}}^N$:$N \times 1$ column vector with $B_{r_{pos}n}^N = \int_0^L b_r(x)\phi_n dx$,

B_d^N : $N \times 1$ column vector with $B_{d_n}^N = \int_0^L g_p(x)\phi_n dx$, $n, j = 1, ..., N$.

The position of the sensor is described by

$C_{l_{pos}}^N$: $1 \times N$ row vector with $C_{l_{pos}n}^N = \int_0^L c_l(x)\phi_n dx$, $n = 1, ..., N$.

In another approximation method, the finite element method with Hermite C^1 basis is applied. The bridge structure is discretized into "N" two-node Euler-Bernoulli beam elements, with element length l^e.

The two-node Euler-Bernoulli beam element has four degree-of-freedoms (DOFs). At each node, there is one DOF of vertical displacement and one DOF of rotation about the mid-line. Let u_i denotes the vertical displacement DOF and θ_i denotes the rotation DOF of the global i^{th} node.

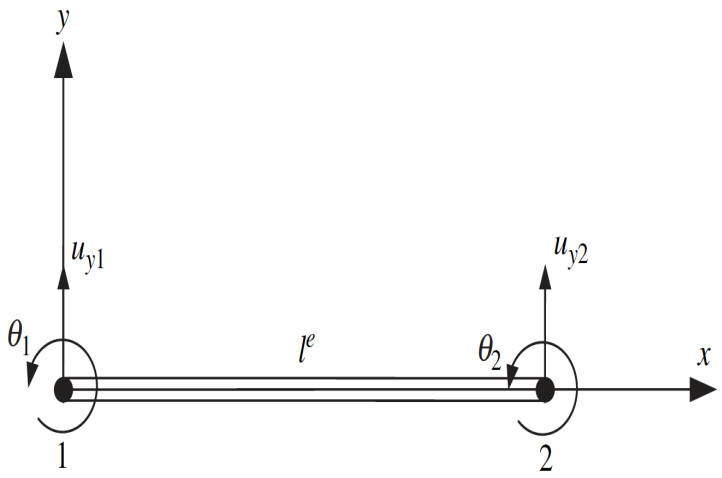

Figure 2.1: A two-node beam element (the subscript y denotes the vertical displacement in the y direction), Figure 10.7 in [15].

Let x_i^n denotes the i^{th} spatial coordinate of the n^{th} element, $n = 1, 2, ..., N$. Let w_b^n denotes the time coefficient (element nodal displacements) vector of the n^{th} element, $w_b^n = [u_1^n, u_2^n, \theta_1^n, \theta_2^n]^T$. Define $\mathcal{H}_n(0, L) = \mathcal{H}_H(0, L) \cap \mathcal{H}_{H_0}(0, L)$, where

$\mathcal{H}_H(0, L) = \{w(x, .) \in \mathcal{H}^2(0, L), w(0, .) = w(L, .) = 0, w'(0, .) = w'(L, .) = 0\}$,

$\mathcal{H}_{H_0}(0, L) = \{\phi \in L_2(0, L) : \phi' \in L_2(0, L), \phi(0) = \phi(L) = 0, \phi'(x) = \phi'(L) = 0\}$.

Choose $\phi_n(x) \in \mathcal{H}_n(0, L)$ to be the Hermite C^1 shape functions. Introduce a change of coordinate variable $\zeta(x) = \frac{2x}{l^e} - 1$ for each element such that the element's domain is in $[-1, 1]$. Let $\phi_n(\zeta(x)) = [\phi_{u1}^n, \phi_{u2}^n, \phi_{\theta 1}^n, \phi_{\theta 2}^n]$, $\zeta \in [-1, 1]$, where

$$\begin{aligned} \phi_{u1}^n &= \frac{1}{4}(1-\zeta)^2(2+\zeta), \\ \phi_{\theta 1}^n &= \frac{l^e}{8}(1-\zeta)^2(1+\zeta), \\ \phi_{u2}^n &= \frac{1}{4}(1+\zeta)^2(2-\zeta), \\ \phi_{\theta 2}^n &= \frac{l^e}{8}(1+\zeta)^2(\zeta-1). \end{aligned} \tag{2.2.3}$$

For each element, the element mass, the element stiffness, the element damping, and the element input matrices are given by

$$\begin{aligned} M^n &= \rho \frac{l^e}{2} \int_{-1}^{1} \phi^{nT} \phi^n d\zeta \\ &= \frac{\rho l^e}{420} \begin{bmatrix} 156 & 54 & 22l^e & -13l^e \\ 54 & 156 & 13l^e & -22l^e \\ 22l^e & 13l^e & 4l^{e2} & -3l^{n2} \\ -13l^e & -22l^e & -3l^{e2} & 4l^{e2} \end{bmatrix}, \end{aligned} \tag{2.2.4}$$

$$\begin{aligned} K^n &= EI \frac{l^e}{2} \int_{-1}^{1} \frac{d^2(\phi^n)}{d\zeta^2}^T \frac{d^2(\phi^n)}{d\zeta^2} d\zeta \\ &= \frac{EI}{(l^e)^3} \begin{bmatrix} 12 & -12 & 6l^e & 6l^e \\ -12 & 12 & -6l^e & -6l^e \\ 6l^e & -6l^e & 4l^{e2} & 2l^{e2} \\ 6l^e & -6l^e & 2l^{e2} & 4l^{e2} \end{bmatrix}, \end{aligned} \tag{2.2.5}$$

$$D^n = \frac{c_d}{\rho} M^n + k_d K^n, \tag{2.2.6}$$

$$B^n_{r_{pos}} = \frac{l^e}{2}\int_{-1}^{1} b_r(x(\zeta))\phi^{nT} d\zeta, \tag{2.2.7}$$

$$B^n_d = \frac{l^e}{2}\int_{-1}^{1} g_p(x(\zeta))\phi^{nT} d\zeta, \tag{2.2.8}$$

$$C^n_{l_{pos}} = \frac{l^e}{2}\int_{-1}^{1} c_l(x(\zeta))\phi^{n} d\zeta. \tag{2.2.9}$$

Then, the element matrices are assembled into the N-elements global mass, the N-elements global stiffness, the N-elements global damping, and the N-elements global input matrices correspondingly. The N-elements second-order system ODEs is

$$M\ddot{w}^N_b(t) + D\dot{w}^N_b(t) + K^N w^N_b(t) = B^N_{r_{pos}} u(t) + B^N_d \omega_p(t), \tag{2.2.10}$$

where w^N_b denote the global nodal displacements, M, D and K are the global finite element mass, damping and stiffness matrices respectively, and $B^N_{r_{pos}}$ and B^N_d are the global input force vectors for the system (2.1.5) (with boundary conditions taken into account). Details in assembling the element matrices into the global matrices can be found in the textbook [15]. Since the procedure is tedious, details will not be shown in the thesis.

In the remaining thesis, the control designs are applied on the modal approximated finite-dimensional system in chapter 4 and on the Hermite basis FEM approximated finite-dimensional system in chapter 5. To keep the approximation state-space form generalized for both approximation methods, the matrices M, D, K $B^N_{r_{pos}}$, B^N_d, and $C^N_{l_{pos}}$ are denoted by the same names for two approximation methods, and the method chosen will be specified to the readers when relevant. Define the finite-dimensional space $\mathcal{Z}_n = \mathcal{H}_n(0, L) \times \mathcal{H}_n(0, L)$, and let $[w^N_b, \dot{w}^N_b]^T \in \mathcal{Z}_n$. Define the sensor position matrix $C^N_{2b_l} = [C^N_{l_{pos}}, 0]$ and define the output from the sensor

$$y_{2b}(t) = C^N_{2b_l} z^N_b(t). \tag{2.2.11}$$

After approximating the system (2.1.5), the system model and measurement output are represented in the state space form

$$\dot{z}^N_b(t) = A^N_b z^N_b(t) + B^N_{2b_r} u(t) + B^N_{1b}\omega_p(t),\ z^N_b(0) = z^N_{b_0} = 0, \tag{2.2.12}$$

$$y_{2b}(t) = C^N_{2b_l} z(t), \tag{2.2.13}$$

where

$$A_b^N = \begin{bmatrix} 0 & I \\ -M^{-1}K & -M^{-1}D \end{bmatrix}, B_{2b_r}^N = \begin{bmatrix} 0 \\ -M^{-1}B_{r_{pos}}^N \end{bmatrix}, B_{1b}^N = \begin{bmatrix} 0 \\ -M^{-1}B_d^N \end{bmatrix}, \quad (2.2.14)$$
$$C_{2b_l}^N = \begin{bmatrix} C_{l_{pos}}^N & 0 \end{bmatrix},$$

and M, D, K, B_{1b}^N, $B_{r_{pos}}^N$ and $C_{l_{pos}}^N$ are the approximation system's mass, damping, stiffness, disturbance, actuator location and sensor location matrices respectively.

In the remaining thesis, the approximation superscript "N" may be dropped.

Chapter 3

Location-Parameterized Linear-Quadratic Controller Designs

In this chapter, a well-known controller design approach, minimizing the infinite time horizon LQ performance index for the control and estimator, is discussed. Theorems of the optimal solutions, the optimal control and the optimal estimator, that minimize the performance index are presented.

The locations of the actuator and sensor affect the optimal control and estimator and consequently affect the controller performance index. Actuator location-parameterized optimal control solution and sensor location-parameterized optimal estimators are presented. Theorems on the existence of optimal locations are provided. The non-collocated and collocated sensor/actuator designed location optimization problems are presented.

The mapping of the performance index, specifically the state weight that weights the energy of the original infinite-dimensional system (2.1.9), from the original functional space to a generic approximation functional space is described in detail.

3.1 Linear-Quadratic Performance Design for Disturbance Systems

Consider a linear system with state $z(t)$, Gaussian disturbance $\omega(t)$, control $u(t)$, and measurement $y_2(t)$ with noise $\nu(t)$:

$$\dot{z}(t) = Az(t) + B_1\omega(t) + B_2u(t),\ z(0) = z_0, \tag{3.1.1}$$
$$y_2(t) = C_2z(t) + D_{21}\nu(t). \tag{3.1.2}$$

The finite-dimensional system, (3.1.1) is defined by vectors and matrices. $z(t) \in \mathbb{R}^n$, $y_2(t) \in \mathbb{R}^q$, $A \in \mathbb{R}^{n\times n}$, $B_2 \in \mathbb{R}^{n\times m}$, $B_1 \in \mathbb{R}^{n\times 1}$, $C_2 \in \mathbb{R}^{q\times n}$,$D_{21} \in \mathbb{R}^{q\times m}$. The disturbance $\omega(t)$ has covariance W, and the sensor noise $\nu(t)$ has covariance R_e. The integers n, m, and q denote the number of states in the system, the number of actuators, and the number of sensors respectively. In this research, $m = q = 1$.

Define the linear-quadratic (LQ) performance index:

$$\begin{aligned} J(u, z_0, T) &= [\frac{1}{2}z^T(T)\Pi_T z(T) + \frac{1}{2}\int_0^T [z(t)^T Qz(t)] + u(t)^T R_u u(t)]dt,\ t \in [0, T], \\ J(u, z_o) &= \lim_{T\to\infty} J(u, z_0, T) = \int_0^\infty z(t)^T Qz(t) + u(t)^T R_u u(t)dt, \end{aligned} \tag{3.1.3}$$

where $Q \in \mathbb{R}^{n\times n}$, $Q \geq 0$, is the state weight, $R_u \in \mathbb{R}^{m\times m}$, $R_u > 0$, is the control weight, and $\Pi_T \in \mathbb{R}^{n\times n}$ is the final state constraint.

In this thesis, the optimal controller is optimal for infinite time, that is, the achieved optimal value of performance is the sum of the performance index over infinite time. The LQ performance control law balances the linear combination of state and control energy spent before the state reaches equilibrium. Mathematically, the objective of the infinite time optimal LQ control $u(t)$ is to minimize $\lim_{T\to\infty} J(u, z_0, T)$, which essentially is a weighted sum of the $\mathcal{L}_2$-norm of the state (transient behaviour criterion) and the control (control criterion) plus a final weighted state, which is zero for the infinite time case [32].

Note that the integrand inside (3.1.3) can also be written in a vector form

$$y_1(t) = C_1z(t) + D_{12}u(t), \tag{3.1.4}$$

where

$$C_1 = \begin{bmatrix} \sqrt{Q} \\ 0 \end{bmatrix}, D_{12} = \begin{bmatrix} 0 \\ \sqrt{R_u} \end{bmatrix}. \tag{3.1.5}$$

Thus, minimizing (3.1.3) is equivalent to

$$\min_u \int_0^\infty \|y_1\|^2 \, dt. \tag{3.1.6}$$

For a partially observed system, an estimator that provides estimation of the full state is needed. Consider a general estimator $\hat{z}$ of the system (3.1.1),

$$\dot{\hat{z}}(t) = A\hat{z}(t) + B_2 u(t) + F(y(t) - C_2\hat{z}(t)), \ \hat{z}(0) = \hat{z}_0, \tag{3.1.7}$$

where F is the estimator gain that needs to be chosen.

The linear-quadratic Estimator (LQE) is an optimal estimator that balances between the weighted reliability of the system model and the weighted reliability of the sensor measured state in a LQ performance index. When the variances of the noises, Gaussian distributed, are known and utilized in the performance index, the LQE becomes the well-known Kalman estimator (Kalman Filter). The Kalman estimator is an optimal estimator that minimizes the error covariance between the estimated state and the actual state. The objective is to minimize the performance index

$$\min_{\hat{z}} \mathbb{E}[\|z(t) - \hat{z}(t)\|^2], \ t \in [0, T], \tag{3.1.8}$$

where $\mathbb{E}[.]$ is the expectation notation.

To solve for the optimal control and estimator in the functional (3.1.3) and (3.1.8), various approaches such as variation of calculus or dynamic programming by optimizing the cost functional under the constraints (3.1.1) to solve for the minimum u and $\hat{z}$ can be applied. Derivations of the solutions and proofs of existence and uniqueness of the optimal control can be found in the work [23], and textbooks [32], [2] and [28].

In this thesis, the controllers are designed following the theorems for output feedback designs. Let $\lambda_i(A)$ denote the i^{th} eigenvalue of an $n \times n$ matrix A. Consider the following definitions:

Definition 1 *If* $\max_{1\leq i\leq n} Re(\lambda_i(A)) < 0$, *then* A *is Hurwitz.*

Definition 2 *The pair (A,B) is stabilizable if there exists* K *such that* $A-BK$ *is Hurwitz.*

Definition 3 *The pair (A,C) is detectable if there exists* F *such that* $A-FC$ *is Hurwitz.*

Theorem 3.1.1 *(Optimal solution u to (3.1.3)): Assume* (A, B_2) *is stabilizable and* (A, C_2) *is detectable. Then the infinite time horizon minimum cost of (3.1.3) exists for each initial condition* z_0. *There exists a symmetric non-negative matrix* Π, *such that:*

$\min_{u\in\mathcal{L}_2(0,\infty;\mathbb{R}^m)} J(z_0, u) = J(z_0, u_{opt}) = z_0^T \Pi z_0$, *where* Π *is the minimal non-negative solution to the Algebraic Riccati Equation (ARE):*

$$A^T\Pi + \Pi A + Q - \Pi B_2 {R_u}^{-1} B_2^T \Pi = 0. \tag{3.1.9}$$

That is, any other (symmetric) solution Π_1 *to the ARE has* $z_0^T \Pi z_0 \leq z_0^T \Pi_1 z_0$, *for all* $z_0 \in \mathbb{R}^n$.

Define the control gain $K = R_u^{-1} B_2^T \Pi$. *The corresponding optimal control is*

$$u_{opt}(t) = -Kz(t), \tag{3.1.10}$$

and $A - B_2K$ *is Hurwitz.*

Hence, by Theorem (3.1.1) , the state-feedback law $u(t) = -Kz(t)$ stabilizes the system and minimizes the LQ performance index (among all stabilizing controllers) with the optimal performance $z_0^T \Pi z_0$.

Consider the following definitions:

Definition 4 *The trace of an* $n \times n$ *square matrix* A *is*

$$Tr(A) = \sum_{i=1}^{n} a_{ii}. \tag{3.1.11}$$

Definition 5 *The trace norm (nuclear norm) of a real matrix A is*

$$\|A\|_1 = Tr(\sqrt{AA^T}). \tag{3.1.12}$$

Theorem 3.1.2 *(Optimal Solution $\hat{z}$ to (3.1.8)): Assume $(A, B_1\sqrt{W})$ is stabilizable and (A, C_2) is detectable. Then the infinite time horizon minimum cost of (3.1.8) exists for all $z \in \mathbb{R}^n$, and there exists a unique symmetric non-negative matrix Σ, such that:*

$\mathbb{E}[\|z(t) - \hat{z}_{opt}(t)\|^2] = \min_{\hat{z}} \mathbb{E}[\|z(t) - \hat{z}(t)\|^2] = \|\Sigma\|_1$,
where Σ is the minimal non-negative solution to the ARE:

$$A\Sigma + \Sigma A^T + B_1 W B_1^T - \Sigma C_2^T R_e^{-1} C_2 \Sigma = 0. \tag{3.1.13}$$

That is, any other solution Σ_1 to the ARE has $\|\Sigma\|_1 \leq \|\Sigma_1\|_1$.

The error covariance

$$\mathbb{E}[(z(t) - \hat{z}_{opt}(t)) \circ (z(t) - \hat{z}_{opt}(t))] = \Sigma. \tag{3.1.14}$$

Define the optimal estimator gain $F = \Sigma C_2^T R_e^{-1}$. The optimal estimator is

$$\dot{\hat{z}}_{opt}(t) = A\hat{z}(t) + B_2 u(t) + F(y_2(t) - C_2\hat{z}(t)),\ \hat{z}(0) = \hat{z}_0, \tag{3.1.15}$$

and $A - FC_2$ is Hurwitz.

The solution to the estimator associated ARE (3.1.13) is the same as the solution to the LQ control assoicated ARE (3.1.9), with $A = A^T, B_2 = C_2^T$, $C_2^T C_2 = B_1 W B_1^T$, $R_u = R_e$. Thus, like the concepts of controllability and observability are dual, the optimization problems of the LQ control and the Kalman estimator are dual.

3.2 Location-Parameterized Controller

In this thesis, the control force is applied at the actuator's location on the structure, and the deflection response is measured at the sensor's location on the structure. Let the possible actuator locations on the structure be the set denoted by Ω_r, and let the possible

sensor locations on the structure be the set denoted by Ω_l.

To consider the dependency on the actuator locations of the input control matrix B_2, let it be actuator location r-parameterized and denoted by B_{2_r}. Similarly, to consider the dependency on the sensor locations of the output measurement matrix C_2, let it be sensor location l-parameterized and denoted by C_{2_l}. Thus, the solutions to the location-parameterized AREs (3.2.1) and (3.2.2) become location dependent: $\Pi = \Pi(r)$ and $\Sigma = \Sigma(l)$. Consequently, the optimal performance index will vary with the locations of the sensor/actuator.

$$A^T\Pi(r) + \Pi(r)A + Q - \Pi(r)B_{2_r}{R_u}^{-1}B_{2_r}^T\Pi(r) = 0, \tag{3.2.1}$$

$$A\Sigma(l) + \Sigma(l)A^T + B_1WB_1^T - \Sigma(l)C_{2_l}^T{R_e}^{-1}C_{2_l}\Sigma(l) = 0, \tag{3.2.2}$$

$$J_{opt}(z_0, u_{opt}(r)) = z_0^T\Pi(r)z_0, \tag{3.2.3}$$

$$\mathbb{E}[\|z(t) - \hat{z}_{opt}(t)\|^2] = \|\Sigma(l)\|_1 . \tag{3.2.4}$$

The following theorems show the existence of the optimal sensor location and the existence of the optimal actuator location for infinite-dimensional systems. The theorems apply to the finite-dimensional problem (3.1.1) as well, where the operator $B(r)$ becomes a matrix B_{2_r}, $C(l)$ becomes a matrix C_{2_l}. Details on the existences of optimal locations of actuator and sensor can be found in works [34] and [50].

Theorem 3.2.1 *(Continuity of $\Pi(r)$ and Existence of an Optimal LQ Actuator Location, Theorem 2.6 [34]) Let $B(r) \in \mathcal{L}(\mathcal{U}, \mathcal{Z})$ be a family of compact input operators such that for any $r_0 \in \Omega_r$,*

$\lim_{r\to r_0} \|B(r) - B(r_0)\| = 0.$

If (A,B(r)) is stabilizable for all $r \in \Omega_r$ and (A, C_1) is detectable, then the Riccati operators $\Pi(r)$ are continuous functions of r in the operator norm:

$\lim_{r\to r_0} \|\Pi(r) - \Pi(r_0)\| = 0,$
and there exists an optimal actuator location $\hat{r}$ such that:

$\|\Pi(\hat{r})\| = \inf_{r\in\Omega_r} \|\Pi(r)\| = \hat{\mu}.$

Theorem 3.2.2 *(Continuity of $\Sigma(l)$ and Existence of an Optimal Sensor Location, Theorem 4.1 [50])*

Assume $\mathcal{W}$ and $\mathcal{Y}$ are finite-dimensional spaces. Let $C(l) \in \mathcal{L}(\mathcal{Z}, \mathcal{Y})$, $l \in \Omega_l$ be a family of output operators such that for any $l_0 \in \Omega_l$,

$\lim_{l \to l_0} \|C(l) - C(l_0)\| = 0.$

If $(A, B_1\sqrt{W})$ is exponentially stabilizable and $(A, C(l))$ is exponentially detectable, then the corresponding Riccati operators $\Sigma(l)$ are continuous functions of l in the nuclear norm:

$\lim_{l \to l_0} \|\Sigma(l) - \Sigma(l_0)\|_1 = 0,$

and there exists an optimal sensor location $\hat{l}$ such that:

$\left\|\Sigma(\hat{l})\right\|_1 = \min_{l \in \Omega_l} \|\Sigma(l)\|_1 = \hat{\mu}_l.$

3.3 Approximation of the State Weight in the Control Performance Index

The LQ performance index is a combination of the weighted state and control effort of the controlled system. Structural control works done by [41] and [1] have revealed that weighting the state proportional to the system's potential energy via the stiffness matrix and proportional to the system's kinetic energy via the mass matrix in the control performance index can efficiently control the response.

However, the controllers are for the finite-dimensional system that approximates the original infinite-dimensional system (2.1.9), so the state weight C_1 in the performance index approximates the original state weight operator. In this section, a mapping is derived for the state weight operator C_1 from the infinite-dimensional space to the finite-dimensional space spanned by the numerical approximation basis.

Recall the separable Hilbert space, $\mathcal{H}_s(0, L) = \{w \in \mathcal{H}^2(0, L), w(0) = 0, w(L) = 0\}$ and the functional space, $\mathcal{Z}_{inf} = \mathcal{H}_s(0, L) \times \mathcal{L}_2(0, L)$ defined in chapter 2.

Define the norm on $\mathcal{H}_s(0, L)$ to be

$$\|w\|_{\mathcal{H}_s} = \|w\|_{\mathcal{H}^2} = \sqrt{\int_0^L |w(x)''|^2 \, dx}. \tag{3.3.1}$$

Define the norm on $\mathcal{Z}_{inf}$ to be

$$\begin{aligned}\|z_p(x,.)\|_{\mathcal{Z}_{inf}} &= \left\| \begin{bmatrix} w(x,t) \\ v(x,t) \end{bmatrix} \right\|_{\mathcal{Z}_{inf}} \\ &= \sqrt{\|w(x,t)\|^2_{\mathcal{H}_s} + \|v(x,t)\|^2_{\mathcal{L}^2}} \\ &= \sqrt{\int_0^L \left| \frac{\partial^2 w(x,t)}{\partial x^2} \right|^2 + |v(x,t)|^2 \, dx}.\end{aligned} \tag{3.3.2}$$

Define an infinite-dimensional state $z_p = [w(x,t), v(x,t)]^T \in \mathcal{Z}_{inf}$.

Define the weighted state as

$$y = C z_p(x,.), \tag{3.3.3}$$

Assume that the operator C is in a block diagonal form such that the weights on $w(.,t)$ and $v(.,t)$ are orthogonal,

$$C = \begin{bmatrix} C_{1_1} & 0 \\ 0 & C_{1_2} \end{bmatrix}. \tag{3.3.4}$$

Choose an approximation basis $\{\phi_n\}_{n=1}^N$, where $n = 1, 2, ..., N$, and N denotes the order of the approximation. Let $\mathcal{H}_n(0,L)$ be the span of ϕ_n. The approximation space is $\mathcal{Z}_n = \mathcal{H}_n(0,L) \times \mathcal{H}_n(0,L)$. Define $z_p^N \in \mathcal{Z}_n$ be the approximation of z_p,

$$z_p^N = \begin{bmatrix} w^N \\ v^N \end{bmatrix} = \begin{bmatrix} \sum_n w_n \phi_n \\ \sum_n v_n \phi_n \end{bmatrix}. \tag{3.3.5}$$

The goal is to find a mapping Ψ for the block diagonal operator C in (3.3.4),

$\Psi : \mathcal{L}(\mathcal{Z}_{inf}, \mathcal{Z}_{inf}) \to \mathcal{L}(\mathcal{Z}_n, \mathcal{Z}_n)$, such that $\Psi(C) = C|_{\mathcal{Z}_n}$.

Since time dimension is not relevant in the context of spatial functional space transformation, the time argument is dropped.

Consider the weighted state in (3.3.3) and denote it by $y(x)$ to indicate the dependency on the spatial variable x,

$$y(x) = Cz_p = \begin{bmatrix} C_{1_1} & 0 \\ 0 & C_{1_2} \end{bmatrix} \begin{bmatrix} w(x,.) \\ v(x,.) \end{bmatrix} = \begin{bmatrix} C_{1_1} w(x,.) \\ C_{1_2} v(x,.) \end{bmatrix}. \tag{3.3.6}$$

The norm of $y(x)$ is

$$\begin{aligned} \|y\|^2_{\mathcal{Z}_{inf}} &=< C_{1_1} w, C_{1_1} w >_{\mathcal{H}_s} + < C_{1_2} v, C_{1_2} v >_{\mathcal{L}_2}, \\ &= \int_0^L [C_{1_1} w'' \overline{C_{1_1} w''} + C_{1_2} v \overline{C_{1_2} v}] dx. \end{aligned} \tag{3.3.7}$$

Consider the approximation (3.3.5) to w and v in (3.3.7),

$$\int_0^L \sum_{m=1}^N \sum_{n=1}^N C_{1_1} w_m \phi_m'' w_n \phi_n'' C_{1_1} dx + \int_0^L \sum_{m=1}^N \sum_{n=1}^N C_{1_2} v_m \phi_m, v_n \phi_n C_{1_2} dx, \tag{3.3.8}$$

and the approximation to (3.3.6), denoted as $\|y_{1n}\|_2^2$ becomes

$$\|y_{1n}\|_2^2 = \begin{bmatrix} \vec{w}_n & \vec{v}_n \end{bmatrix} \begin{bmatrix} K_p(C_{1_1}) & 0 \\ 0 & M_k(C_{1_2}) \end{bmatrix} \begin{bmatrix} \vec{w}_n \\ \vec{v_n} \end{bmatrix}, \tag{3.3.9}$$

where $K_p(C_{1_1})$, $M_k(C_{1_2})$ are $N \times N$ matrices with entries

$$K_{p_{n,m}}(C_{1_1}) = \int_0^L C_{1_1}^2 \phi_n'' \phi_m'' dx, \tag{3.3.10}$$

$$M_{k_{n,m}}(C_{1_2}) = \int_0^L C_{1_2}^2 \phi_n \phi_m dx, \tag{3.3.11}$$

for n,$m = 1, 2, ..., N$,
and $\vec{w}_n = [w_1, ..., w_N] \in \mathbb{R}^N$, $\vec{v}_n = [v_1, ..., v_N] \in \mathbb{R}^N$ are the vectors of approximation coefficients in (3.3.5). Rewrite (3.3.9) as

$$\|y_{1n}\|_2^2 = \begin{bmatrix} \vec{w}_n^T & \vec{v}_n^T \end{bmatrix} \begin{bmatrix} \sqrt{K_p(C_{1_1})} & 0 \\ 0 & \sqrt{M_k(C_{1_2})} \end{bmatrix}^T \begin{bmatrix} \sqrt{K_p(C_{1_1})} & 0 \\ 0 & \sqrt{M_k(C_{1_2})} \end{bmatrix} \begin{bmatrix} \vec{w}_n \\ \vec{v_n} \end{bmatrix}, \tag{3.3.12}$$

and define the matrix $C_n = \begin{bmatrix} \sqrt{K_p(C_{1_1})} & 0 \\ 0 & \sqrt{M_k(C_{1_2})} \end{bmatrix}$, $C_n = C|_{\mathcal{Z}_{inf}}$.

Thus, the mapping Ψ for the block diagonal operator C in (3.3.4) is

$$\Psi(C) = \begin{bmatrix} \sqrt{K_p(C_{1_1})} & 0 \\ 0 & \sqrt{M_k(C_{1_2})} \end{bmatrix}. \tag{3.3.13}$$

When ϕ_n is an orthogonal basis, as in the modal approximation case, the matrices K_p and M_k become diagonal matrices, with $K_{p_{i,i}} = \int_0^L C_{1_1}^2(\phi_i'')^2 dx$, $M_{k_{i,i}} = \frac{L}{2}C_{1_2}^2$, for $i = 1, ..., N$.

An energy-weighted state z_b in (2.1.9) can be expressed in the form of (3.3.6), with C_{1_1} being the weight on the potential energy and C_{1_2} being the weight on the kinetic energy. For constant potential energy weight C_{1_1} and constant kinetic energy weight C_{1_2}, (3.3.13) becomes

$$\Psi(C) = \begin{bmatrix} C_{1_1}K^I & 0 \\ 0 & C_{1_2}M^I \end{bmatrix}, \tag{3.3.14}$$

where

$$K^I_{n,m} = \sqrt{\int_0^L \phi_n''\phi_m'' dx}, \tag{3.3.15}$$

and

$$M^I_{n,m} = \sqrt{\int_0^L \phi_n\phi_m dx}. \tag{3.3.16}$$

The matrices K^I and M^I in Ψ are the mass and stiffness matrices with unit physical parameters in the numerical approximations.

Chapter 4

A Preliminary Problem

In this chapter, a simplified model of the system (2.1.5) is studied. The modal approximation has been used. The model is a unit parameterized simply supported Euler-Bernoulli beam with random initial condition, and it is subjected to white Gaussian temporal noises. The LQ optimal controller is applied to control the initial condition response and the Gaussian disturbance response. The controller combines an actuator location-parameterized LQ control law, and a sensor location-parameterized Kalman estimator. The collocated and non-collocated sensor/actuator controller designs are considered in this chapter. Numerical implementations are presented, and numerical challenges are discussed and provided with resolutions. Optimization on locations with different state weights and disturbances are calculated to study the changes in controlled responses and optimal locations.

4.1 Simple Preliminary Model Control

Let $w_u(x,t)$ denote the deflection and $m_u(x,t)$ denote the moment of the simply supported Euler-Bernoulli beam of unit length, $L = 1$, at position x and time t. Let the Kelvin-Voigt damping be 0.0001.

$$\begin{aligned}\frac{\partial^2 w_u(x,t)}{\partial t^2} + 0.0001\frac{\partial^5 w_u(x,t)}{\partial t \partial x^4} + \frac{\partial^4 w_u(x,t)}{\partial x^4} &= b_r(x)u(t) + g_i(x)\omega_1(t),\\ w_u(0,t) = 0 = w_u(1,t),&\\ m_u(0,t) = 0 = m_u(1,t),&\\ w_u(x,0) = w_{u0}(x),\ \frac{\partial w_u(x,0)}{\partial t} &= v_{u0}(x),\\ x \in [0,1], t \geq 0.&\end{aligned} \tag{4.1.1}$$

The disturbance to the system has bounded spatial distribution $g_i(x) \in \mathcal{L}_2(0,1)$ and temporal Gaussian disturbance $\omega_1(t)$. The control force is applied at the location r, characterized by $b_r(x)$ in (2.1.6).

Define the state $z_u(t) = \begin{bmatrix} w_u(x,t) \\ \dot{w}_u(x,t) \end{bmatrix} \in \mathcal{Z}_{inf}$, the state-space form of (4.1.1) is

$$\dot{z}_u(t) = A_u z_u(t) + B_{2u_r} u(t) + B_{1u}\omega_1(t),\ z_u(0) = z_{u_0}, \tag{4.1.2}$$

where

$$A_u z_u = \begin{bmatrix} \dot{w}_u(x,t) \\ -0.0001\frac{\partial^5 w_u(x,t)}{\partial t \partial x^4} - \frac{\partial^4 w_u(x,t)}{\partial x^4} \end{bmatrix}, B_{2u_r} = \begin{bmatrix} 0 \\ br(x) \end{bmatrix}, B_{1u} = \begin{bmatrix} 0 \\ g_i(x) \end{bmatrix},$$

with domain

$$dom(A_u) = \{z_u \in \mathcal{Z}_{inf} | z_{u1}'' + 0.0001 z_{u2}'' \in \mathcal{H}_s(0,1)\}.$$

Using modal approximation on the first 10 modes, $N = 10$, let $(A_u^N, [B_{2u_r}^N, B_{1u}^N], C_{2u_l}^N)$ be the modal approximated system. The matrix $B_{2u_r}^N$ is actuator location r-parameterized and the matrix $C_{2u_l}^N$ is sensor location l-parameterized. This leads to

$$\dot{z}_u^N(t) = A_u^N z_u^N(t) + B_{2u_r}^N u(t) + B_{1u}^N \omega_1(t),\ z_u^N(0) = z_{u0}^N, \tag{4.1.3}$$

$$y_{2u}(t) = C_{2u_l}^N z_u^N(t) + \nu_1(t), \tag{4.1.4}$$

where $y_{2u}(t)$ is the sensor output of the deflection at the location l, characterized by $c_l(x)$ in (2.1.12) and $\nu_1(t)$ is white Gaussian sensor noise.

The LQG method is an output feedback design for a stochastic system with Gaussian distributed disturbances, i.e. z_0, $\omega_1(t)$ and $\nu_1(t)$ in (3.1.1) are Gaussian random variables (R.V.s). The LQG design uses the Kalman estimator's estimated state to design an LQ state feedback law.

The sensor/actuator location-parameterized LQG controller design will be applied to the preliminary problem. The superscript "N" denoting the approximated system will be dropped. Define the LQ control performance index:

$$J(u, z_0) = \int_0^\infty z_u(t)^T Q z_u(t) + u(t)^T R u(t) dt, \tag{4.1.5}$$

where $Q \geq 0$ being the state weight, and $R > 0$ being the control weight.

Define the Kalman estimator $\hat{z}_u$ performance index:

$$J_K(\hat{z}_u) = \mathbb{E}[\|\hat{z}_u - z_u\|^2]. \tag{4.1.6}$$

To obtain the optimal LQG controller, the state feedback control and the estimator can be designed separately and then combined together. The sensor/actuator location-parameterized LQG implies that the optimal control and optimal estimator are dependent on the actuator and sensor location. The following theorem formally states that the output feedback can be decoupled completely into a non-noisy state feedback design and an estimator design. Textbooks such as [39], [2], [32] state and/or prove the formal theorem.

Theorem 4.1.1 *(Stochastic Separation Theorem for LQG Design)[39] The optimal LQG control of the system (3.1.1), with the control cost functional (3.1.3) and estimator cost functional (3.1.8), is obtained by taking the optimal control law $u_k(t) = -Kz(t)$, where $K = -R_u^{-1} B_2^T \Pi$, and Π is the minimal non-negative solution to the deterministic Algebraic Riccati Equation (ARE) (3.1.9), and replace z with the optimal estimator $\hat{z}(t) = z(t) - e(t)$, yielded by the optimal Kalman filter $F = -\Sigma C_2^T R_e^{-1}$, where Σ is the minimal non-negative solution to the Algebraic Riccati Equation (ARE) (3.1.13).*

The optimal controller is

$$\begin{aligned} \dot{\hat{z}}(t) &= [A - FC_2 - B_2 K]\hat{z}(t) + F y_2(t),\ \hat{z}(0) = \hat{z}_0 = E\{z_0\} \\ u^*(t) &= -K\hat{z}(t). \end{aligned} \tag{4.1.7}$$

The closed-loop control system of (3.1.1) *coupling with the optimal controller* (4.1.7) *has eigenvalues:*

$$\lambda(A - B_2K) \cup \lambda(A - FC_2). \tag{4.1.8}$$

Such a synthesis is therefore decomposed in two independent problems:

- optimization of the control of the deterministic plant.
- optimization of the estimation of the state z from the plant measurements y.

The optimal LQG controller achieves the minimal performance index [21]:

$$\begin{aligned} J_{opt} &= lim_{t\to\infty} E[z^T(t)Qz(t) + u(t)^T R_u u(t)] \\ &= Tr(\Pi B_1 W {B_1}^T + \Sigma K^T R_u K). \end{aligned} \tag{4.1.9}$$

The location-parameterized LQG controller for the preliminary problem (4.1.3) becomes

$$\begin{aligned} &\dot{\hat{z}}_u(t) = [A_u - F_{u_l}C_{2u_l} - B_{2u_r}K_{u_r}]\hat{z}_u(t) + F_{u_l}y_{2u}(t),\ \hat{z}_u(0) = \hat{z}_{u_0}, \\ &u^*(t) = -K_{u_r}\hat{z}_u(t), \end{aligned} \tag{4.1.10}$$

where $K_{u_r} = R^{-1}B_{2u_r}^T\Pi_{u_r}$, and Π_{u_r} is the minimal non-negative solution to the actuator location-parameterized ARE (3.2.1) with $A = A_u$, $B_{2_r} = B_{2u_r}$, $R_u = R$.

$F_{u_l} = \Sigma_{u_l}C_{2u_l}^T V^{-1}$, where Σ_{u_l} is the minimal non-negative solution to the sensor location-parameterized ARE (3.2.2), with $A = A_u$, $B_1 = B_{1u}$, $C_{2_l} = C_{2u_l}$, $R_e = V$.

For the optimal infinite time horizon performance index at location (l, r), the optimal LQG performance index value is

$$Tr(\Pi_{u_r}B_{1u}WB_{1u}^T + \Sigma_{u_l}K_{u_r}^T RK_{u_r}). \tag{4.1.11}$$

The sensor/actuator location optimization cost functional is defined as

$$J^*(l, r) := Tr(\Pi_{u_r}B_{1u}WB_{1u}^T + \Sigma_{u_l}K_{u_r}^T RK_{u_r}). \tag{4.1.12}$$

For the non-collocated sensor/actuator design, define $\Omega_s := \{(l, r) \in \Omega_l \times \Omega_r\}$ as the set of possible sensor/actuator location pairs.

For the collocated sensor/actuator design, define $\Omega_c := \{r_c \in \Omega_r\}$ as the set of possible collocated sensor/actuator locations.

The non-collocated sensor/actuator location optimization problem is to find $(l, r) \in \Omega_s$ that minimizes the cost functional (4.1.12). The objective is

$$\min_{(l,r)\in\Omega_s} J^*(l, r). \tag{4.1.13}$$

Define the optimal locations of the non-collocated sensor/actuator as

$$(l^*, r^*) = argmin J^*(l, r). \tag{4.1.14}$$

The collocated sensor/actuator location optimization problem is to find $r_c \in \Omega_c$ that minimizes the cost functional (4.1.12). The objective is

$$\min_{r_c\in\Omega_c} J^*(r_c, r_c). \tag{4.1.15}$$

Define the optimal locations of the collocated sensor/actuator as

$$r_c^* = argmin J^*(r_c(1, 1)). \tag{4.1.16}$$

4.2 Numerical Implementations

The closed loop formed by the plant with realization $(A, [B_1, B_2], [C_1, C_2], [D_{12}, D_{21}])$ and the controller with realization $(A - FC_2 - B_2K, F, -K, 0)$ is implemented in Matlab:

$$\begin{bmatrix} \dot{z} \\ \dot{\hat{z}} \end{bmatrix} = \begin{bmatrix} A & -B_2K \\ FC_2 & A - FC_2 - B_2K \end{bmatrix} \begin{bmatrix} z \\ \hat{z} \end{bmatrix} + \begin{bmatrix} B_1 & 0 \\ 0 & F \end{bmatrix} \begin{bmatrix} \omega_1(t) \\ \nu_1(t) \end{bmatrix}, \tag{4.2.1}$$

$$\begin{bmatrix} y \\ \hat{y} \end{bmatrix} = \begin{bmatrix} C_2 & 0 \\ 0 & C_2 \end{bmatrix} \begin{bmatrix} z \\ \hat{z} \end{bmatrix} + \begin{bmatrix} D_{21} \\ D_{21} \end{bmatrix} \begin{bmatrix} \omega_1(t) \\ \nu_1(t) \end{bmatrix}. \tag{4.2.2}$$

The Gaussian disturbance is generated by the Matlab function "randn", which gives a Gaussian distributed random number with zero-mean and unit variance. That is, $randn \sim \mathcal{N}(0,1)$.

Any non-Gaussian stochastic disturbance and noise in the system in this thesis are generated by the "randn" function with a shaping filter and scaling by the noise variance.

The approximated system A_n matrix involves the inverse of the mass matrix "M", which often cause numerical difficulties, especially in the Hermite basis FEM simulations. Thus, the descriptor form of the Hermite basis FEM approximation state system with state $z_b^N(t)$ is used. The descriptor form is in the form

$$M^o \dot{z}_b^N(t) = A^o z_b^N(t) + B_1^o \omega_1(t) + B_2^o u(t), \tag{4.2.3}$$

where

$$M^o = \begin{bmatrix} I & 0 \\ 0 & M \end{bmatrix}, A^o = \begin{bmatrix} 0 & I \\ -K & -D \end{bmatrix}, B_1^o = \begin{bmatrix} 0 \\ B_d^N \end{bmatrix}, B_2^o = \begin{bmatrix} 0 \\ B_{r_{pos}}^N \end{bmatrix}, \tag{4.2.4}$$

and where M, D, K, B_d^N, and $B_{r_{pos}}^N$ are the mass, damping, stiffness, disturbance input and actuator location matrices obtained by approximation method. Note that $M^o = M^{oT}$.

The AREs to be solved become

$$A^{oT}\Pi M^o + M^o \Pi A^o + C_1^T C_1 - M^o \Pi B_2^o R_u^{-1} B_2^{oT} \Pi M^o = 0, \tag{4.2.5}$$

$$A^o \Sigma M^o + M^o \Sigma A^{oT} - M^o \Sigma C_2^T R_e^{-1} C_2 \Sigma M^o + B_1^o W B_1^{oT} = 0. \tag{4.2.6}$$

Matlab "icare" function calculates the solution Π and Σ to the above AREs.

Usually, the approximated beam system's operator A_n is ill-conditioned in numerical simulations, so a similarity transformed system is implemented, the energy realization.

The energy realization has state $\tilde{z}_p$ whose elements are moment $m(x,t)$ and velocity $\dot{w}(x,t)$. The state is approximated by

$$\begin{aligned}\tilde{z_p}^N &= [m_n, \dot{w}_n]^T, \\ &= [EIw_n(t)\Phi(x)'' + k_d I\dot{w}_n(t)\Phi(x)'', \dot{w}(t)\Phi(x)]^T.\end{aligned} \tag{4.2.7}$$

Consider the state transformation, $\tilde{z}_p^N = T^{-1}z_p^N$.
Define the transformation matrices

$$\begin{aligned}T^{-1} &= \begin{bmatrix}(\sqrt{EI}\frac{\partial^2}{\partial x^2}) & (\sqrt{k_d I}\frac{\partial^2}{\partial x^2}) \\ 0 & I\end{bmatrix} = \begin{bmatrix}\sqrt{K_{stiff}} & \sqrt{K_{kvd}} \\ 0 & I\end{bmatrix}, \\ T &= \begin{bmatrix}\sqrt{K_{stiff}} & \sqrt{K_{kvd}} \\ 0 & I\end{bmatrix}^{-1},\end{aligned} \tag{4.2.8}$$

where

$$\begin{aligned}K_{stiff_{n,m}} &= \int_0^L EI\phi_n''\phi_m''dx, \\ K_{kvd_{n,m}} &= \int_0^L k_d I\phi_n''\phi_m''dx.\end{aligned} \tag{4.2.9}$$

Let $\tilde{A}_n = T^{-1}A_nT$, $\tilde{B}_1 = T^{-1}B_1$, $\tilde{B_{2_r}} = T^{-1}B_{2_r}$, and $\tilde{C_{2_l}} = C_{2_l}T$.

The transformed state system becomes

$$\dot{\tilde{z}}_p^N(t) = \tilde{A}_n\tilde{z_p}^N(t) + \tilde{B}_1\omega_1(t) + \tilde{B_{2_r}}u(t),\ \tilde{z_p}^N(0) = T^{-1}z_p^N(0) = \tilde{z_{p0}}^N, \tag{4.2.10a}$$

$$\tilde{y}(t) = \tilde{C_{2_l}}\tilde{z_p}^N(t) + \nu_1(t). \tag{4.2.10b}$$

The condition number of $\tilde{A}_n$ in the transformed energy realization and the condition number of A^o in the descriptor realization are reduced. To illustrate this, modal approximation and Hermite basis FEM approximation to the operator A_u in (4.1.2) are calculated in Matlab, and the ratios between the matrix condition numbers of the approximation to A_u to the transformed realization approximations are presented.

Let A_u^N be the numerical approximation to the state-space operator A_u of (4.1.2). Denote its condition number as $cond(A_u^N)$. Denote the energy transformed A_u^N as $\tilde{A}_n = T^{-1}A_u^N T$ (T, T^{-1} defined in (4.2.8)) and its condition number as $cond(\tilde{A}_n)$. Table 4.1 illustrates the increasing relationships between the ratio $\frac{cond(A_u^N)}{cond(\tilde{A}_n)}$ and the number of elements ne and modes N used in the Hermite basis FEM approximation (named FEM-H in the table) and modal approximation. The ratio increases faster as the number of modes N increases in the modal approximation, but increases slower as the number of elements ne increases in the FEM-H approximation.

Table 4.1: Ratio between the condition number of Hermite FEM approximated A_u^N to the condition number of $\tilde{A}_n = T^{-1}A_u^N T$ (Ratio H) increases as number of elements ne increases and
ratio between the condition number of modal approximated A_u^N to the condition number of $\tilde{A}_n = T^{-1}A_u^N T$ (Ratio M) increases as number of modes N increases.
A_u^N: the numerical approximation to the state-space operator A_u of (4.1.2);
$\tilde{A}_n$: the energy transformed matrix $\tilde{A}_n = T^{-1}A_u^N T$ (T and T^{-1} in (4.2.8));
ne: the number of finite elements used in the Hermite basis FEM approximation;
N: the number of modes used in the modal approximation.

FEM-H ne	Ratio (H)	Modal N	Ratio (M)
1	3.4613	1	80.1264
3	13.7436	3	337.3822
9	44.7374	9	109.6616

Denote the descriptor form of A_u^N as $A^o = M^o A_u^N$ (M^o in (4.2.4)) and its condition number as $cond(A^o)$. Table 4.2 illustrates the increasing relationships between the ratio $\frac{cond(A_u^N)}{cond(A^o)}$ and the number of elements ne and modes N used in Hermite basis FEM approximation and modal approximation. The ratio increases steeply as as the number of elements ne increases in FEM-H approximation, but it stays constant as the number of modes N increases in the modal approximation.

Table 4.2: Ratio between the condition number of Hermite FEM approximated A_u^N to the condition number of $A^o = M^o A_u^N$ (Ratio H) increases as number of elements ne increases and
ratio between the condition number of modal approximated A_u^N to the condition number of $A^o = M^o A_u^N$ (Ratio M) stays constant as number of modes N increases.
A_u^N: the numerical approximation to the state-space operator A_u of (4.1.2);
A^o: the descriptor form $A^o = M^o A_u^N$ (M^o in (4.2.4));
ne: the number of finite elements used in the Hermite basis FEM approximation;
N: the number of modes used in the modal approximation.

FEM-H ne	Ratio (H)	Modal N	Ratio (M)
1	420	1	2
3	428.4462	3	2
9	2096	9	2

4.3 Simulation Results of the Location Optimization Problem on the Beam

In this section, the effects of different state weights and different spatial disturbances on the optimal sensor/actuator locations are studied. The advantage of weighting heavily on the velocity states is shown. An association between the optimal locations moving away from the centers of the beam and the scale of the location optimization cost functional range is observed.

The parameters and the state weights used in the simulations are given in Table 4.3 and Table 4.4 correspondingly on the next two pages. The spatial disturbances used in the simulations are shown in Figure 4.1. The sets of possible sensor/actuator locations Ω_l, Ω_r are 50 equally-spaced points on the beam from $\frac{\Delta}{2}$ to $L - \frac{\Delta}{2}$, where L and Δ are the beam length and sensor/actuator width.

The optimization problem is to calculate the values of the cost functional at each sensor/actuator location by iterating all the possible sensor/actuator locations, and then find the sensor/actuator locations that yield the minimal cost functional. Algorithm 1 on the next page describes the pseudo-code of the numerical optimization method.

Algorithm 1 Location optimization pseudo-code

for $r \in \Omega_r$ **do**
  for $l \in \Omega_l$ **do**
    Compute $J^{(l,r)} = J^*(l, r)$
  end for
end for

return
$(l^*, r^*) = min\{min\{J\}\}$
$r_c^* = min\{diag(J)\}$

Table 4.3: Simple Model Parameter Values

Symbol	Descriptive Name	Value
L	Beam Length (m)	1
ρ	Beam Density (kg/L)	1
E	Young's Modulus (G.Pa)	1
I	Moment of Inertia (mm^4)	1
k_d	Kelvin-Voigt Damping	0.0001
V	Sensor Noise	0.002
W	Disturbance Noise	1
R	Control Weight	1
g_1	Uniform Spatial distributions	$g_1(x) = 1$
g_2	Large Peak Spatial distributions	$g_2(x) = 200sech(100(x - 0.35)) + 0.5$

Table 4.4: Simple Model State Weights

Notation	Descriptive Name	Value
α	Weight Conservation Factor	$\frac{2}{11}$
C_{1e}	Unit Weight Full State	$[1, 1, ..., 1] \in \mathbb{R}^{2N}$
C_{1d}	Weight Deflection	$[10\alpha, ..., 10\alpha, \alpha, ..., \alpha] \in \mathbb{R}^{2N}$
C_{1v}	Weight Velocity	$[\alpha, ..., \alpha, 10\alpha, ..., 10\alpha] \in \mathbb{R}^{2N}$
Q	Full State Weight Scaled by q_I	$Q = q_I I \in \mathbb{R}^{2N \times 2N}$
q_I	Scalars on Q	$q_I = 0.01, 1, 100$

The graphs of the performance index vs. collocated sensor/actuator location are shown in Figure 4.2. An increase in the state weight from $Q = 0.01I$ to $Q = 1I$ with uniform disturbance $g_1(x)$ flattens the collocated sensor/actuator performance index graph J^* vs. r_c. An increase in the disturbance from $g_1(x)$ to $g_2(x)$ with $Q = I$ results in the collocated sensor/actuator optimal locations moving away from the centers. An increase in the state weight from $Q = I$ to $Q = 100I$ with large peak disturbance $g_2(x)$ results in the collocated sensor/actuator optimal locations converging to the peak location $x = 0.35$. The graphs of the performance index vs. non-collocated sensor/actuator locations are shown in Figure 4.3. An increase in the state weight from $Q = 0.01I$ to $Q = 1I$ with uniform disturbance $g_1(x)$ results in the actuator's optimal locations being less unique around the centers. An increase in the disturbance from $g_1(x)$ to $g_2(x)$ with $Q = I$ results in both of the sensor/actuator optimal locations being away from the centers. An increase in the state weight from $Q = I$ to $Q = 100I$ with large peak disturbance $g_2(x)$ results in the sensor's optimal locations converging to the peak location $x = 0.35$ and in the center being non-optimal especially in the sensor location dimension (results in a lighter blue, higher performance index, around $l = 0.5$ in the contour plot on the bottom right in Figure 4.3). In both designs, the scale of the performance index range is increased when Q and g_i are larger. A larger Q magnifies the state response and reduces the control effort in the performance index; moving away from the centers enables the control to apply on more modes' anti-nodes of the state. Similarly, the spatial disturbance $g_i(x)$ impacts the optimal locations of the sensor just as the state weight impacts the optimal locations of the actuator. A large peak disturbance $g_2(x)$ causes the optimal locations of the sensor to move away from the centers of the beam and closer toward the peak of $g_2(x)$. The scale of the location optimization cost functional range is also associated with the performances of control responses. As shown in Figure 4.4, by distributing the state weight heavily on the velocity, the scale of the location optimization cost functional range becomes larger and the middle of the beam becomes non-optimal. The controlled response is improved significantly. On

the other hand, by distributing the state weight more on the deflection, the scale of the location optimization cost functional range becomes smaller and the middle of the beam becomes optimal. The controlled responses initially have the largest maximum amplitudes compare to the velocity weight and uniform weight cases.

The optimal actuator locations of the non-collocated design and of the collocated design are always the same. The potential difference between the two designs lies in the non-collocated sensor's optimal locations. When the scale of the location optimization cost functional range is relatively big, the optimal locations of the non-collocated sensor move further away from the center and the performance index at the optimal locations is relatively smaller than the performance index at the collocated optimal locations. The controlled responses appear to be similar. When the scale of the location optimization cost functional range is relatively small, the non-collocated and collocated designs are the same. The influence of $g_i(x)$ on the differences in the non-collocated sensor/actuator and the collocated sensor/actuator designs are shown in Figure 4.5. An increase in the disturbance from $g_1(x)$ to $g_2(x)$ results in the non-collocated sensor's optimal location l^* being further away from the center than the two designs' same actuator's optimal location. In $g_1(x)$ case, the two designs' optimal sensor/actuator locations are exactly the same. In $g_2(x)$ case, the optimally located non-collocated sensor/actuator design performance index is relatively 2% less to the optimally located collocated sensor/actuator design performance index, yielding a maximum deflection response that is relatively 1.3% less and an insignificant difference in control feedback.

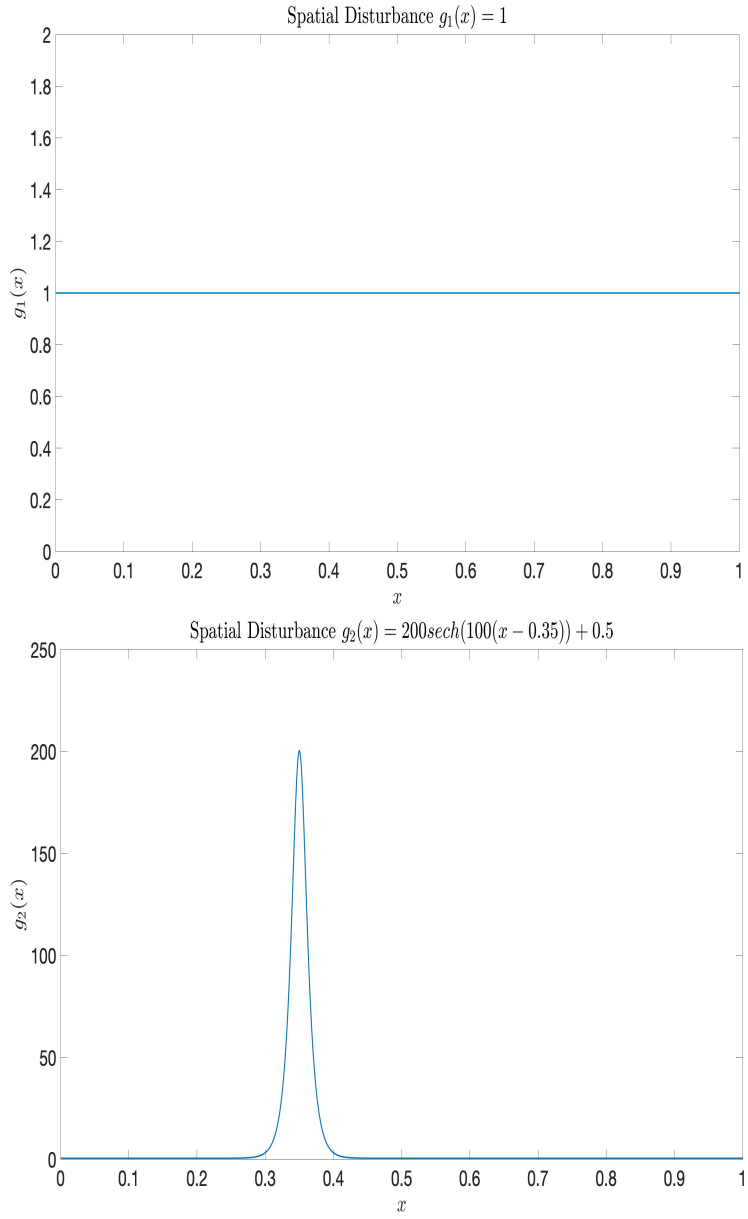

Figure 4.1: Spatial disturbances.
Top: uniform disturbance, $g_1(x) = 1$.
Bottom: large peak disturbance at $x = 0.35$, $g_2(x) = 200sech(100(x - 0.35)) + 0.5$.

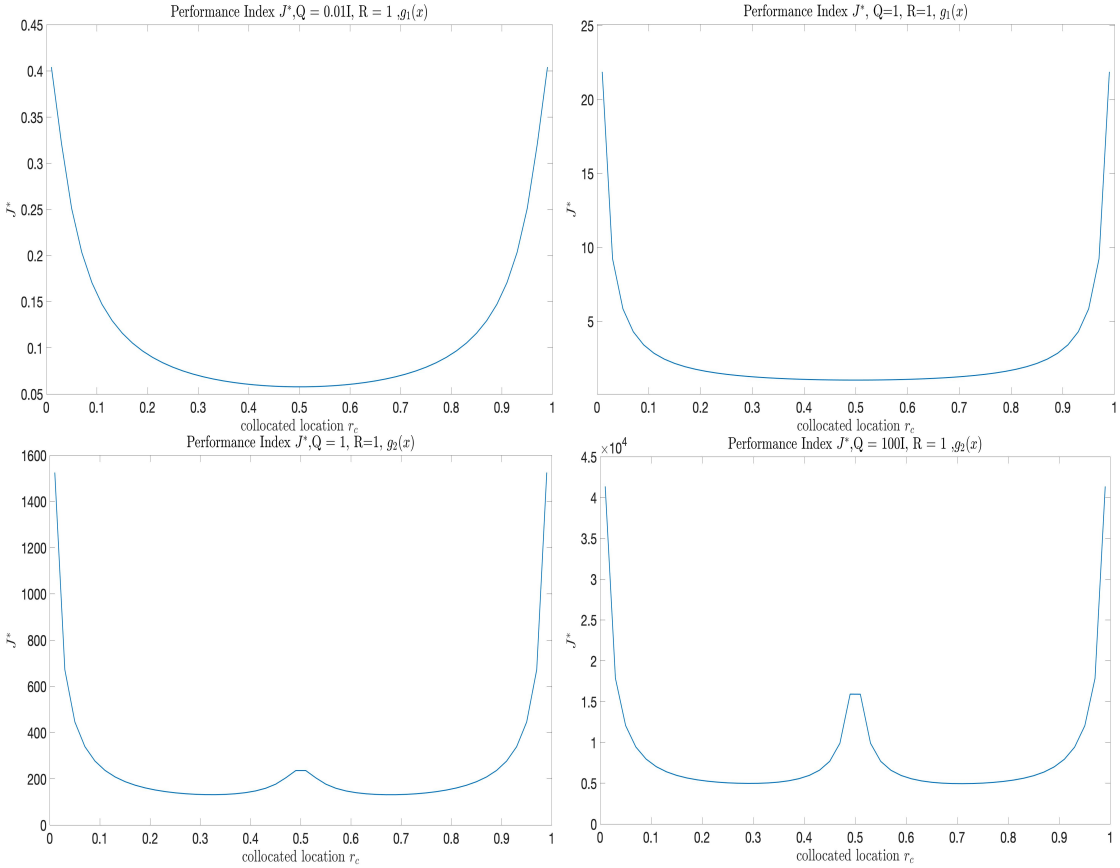

Figure 4.2: Performance index vs. collocated sensor/actuator locations.
Top left: $Q = 0.01I, g_1(x)$, top right: $Q = I, g_1(x)$,
bottom left: $Q = I, g_2(x)$, bottom right: $Q = 100I, g_2(x)$.
Compare effects of the state weights and $g_i(x)$ on the shape of the graph J^* vs. collocated locations.

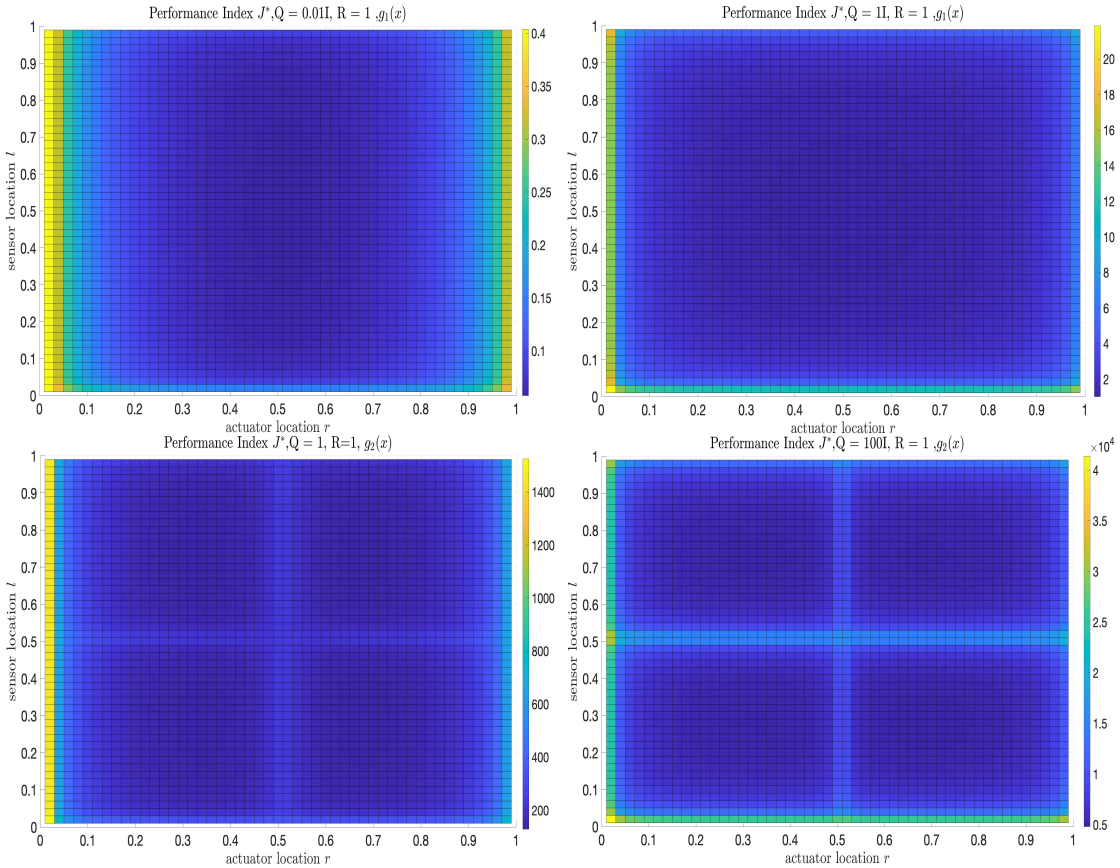

Figure 4.3: Performance index vs. non-collocated sensor/actuator locations.
Top left: $Q = 0.01I, g_1(x)$, top right: $Q = I, g_1(x)$,
bottom left: $Q = I, g_2(x)$, bottom right: $Q = 100I, g_2(x)$.
Compare effects of state weights and $g_i(x)$ on the graph J^* vs. non-collocated locations.

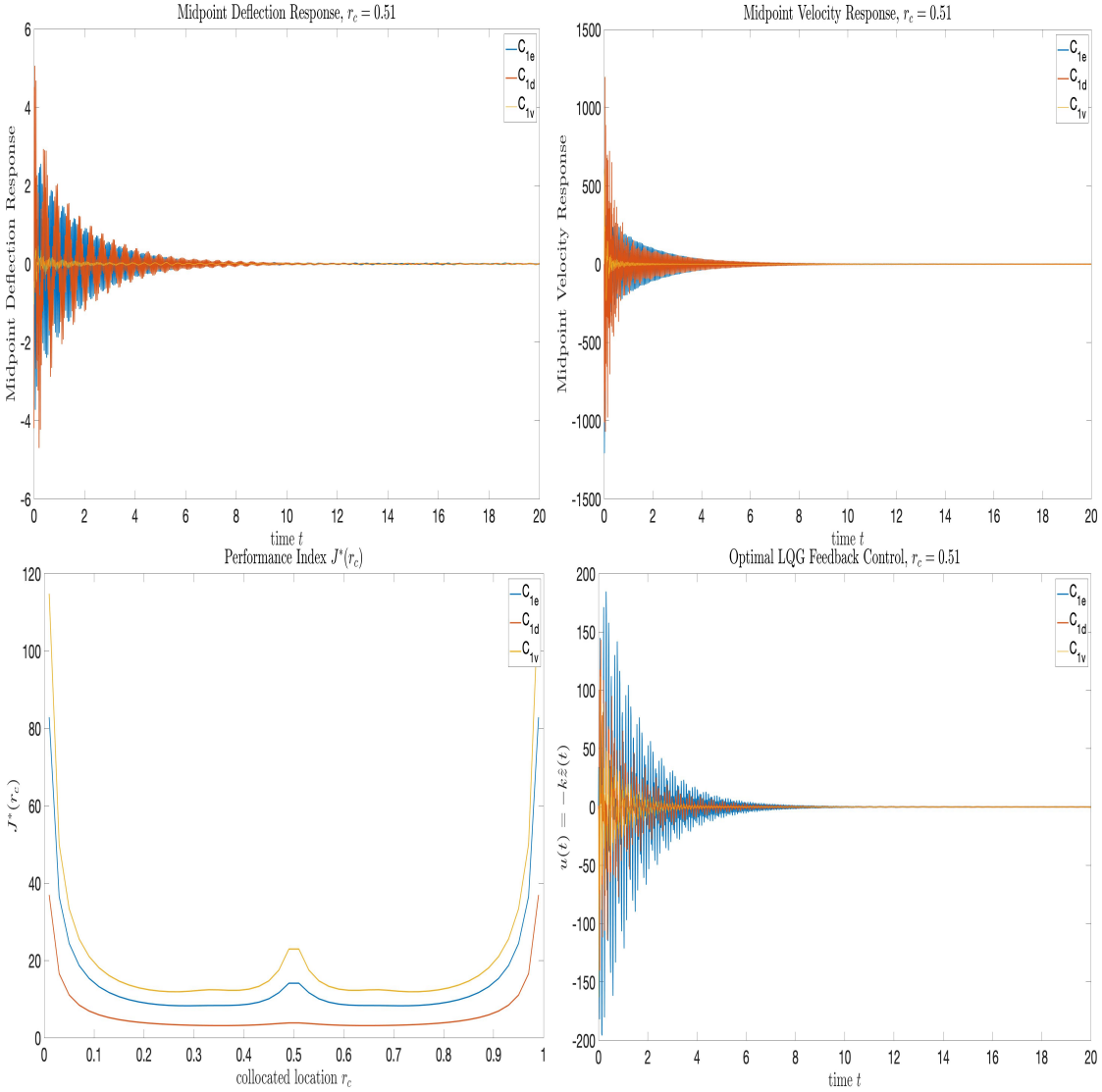

Figure 4.4: Performances at fixed sensor/actuator location $r_c = 0.51L$, random initial condition z_{u_0} with 0 mean and unit variance, uniform disturbance $g_1(x)$, weights C_{1e} (blue), C_{1v} (yellow), C_{1d} (red).
Compare performances of midpoint deflection (top left), midpoint velocity (top right), performance index (bottom left) and LQG feedback $u(t)$ (bottom right) of weighting heavily on deflection, velocity and all states (units normalized by mass).

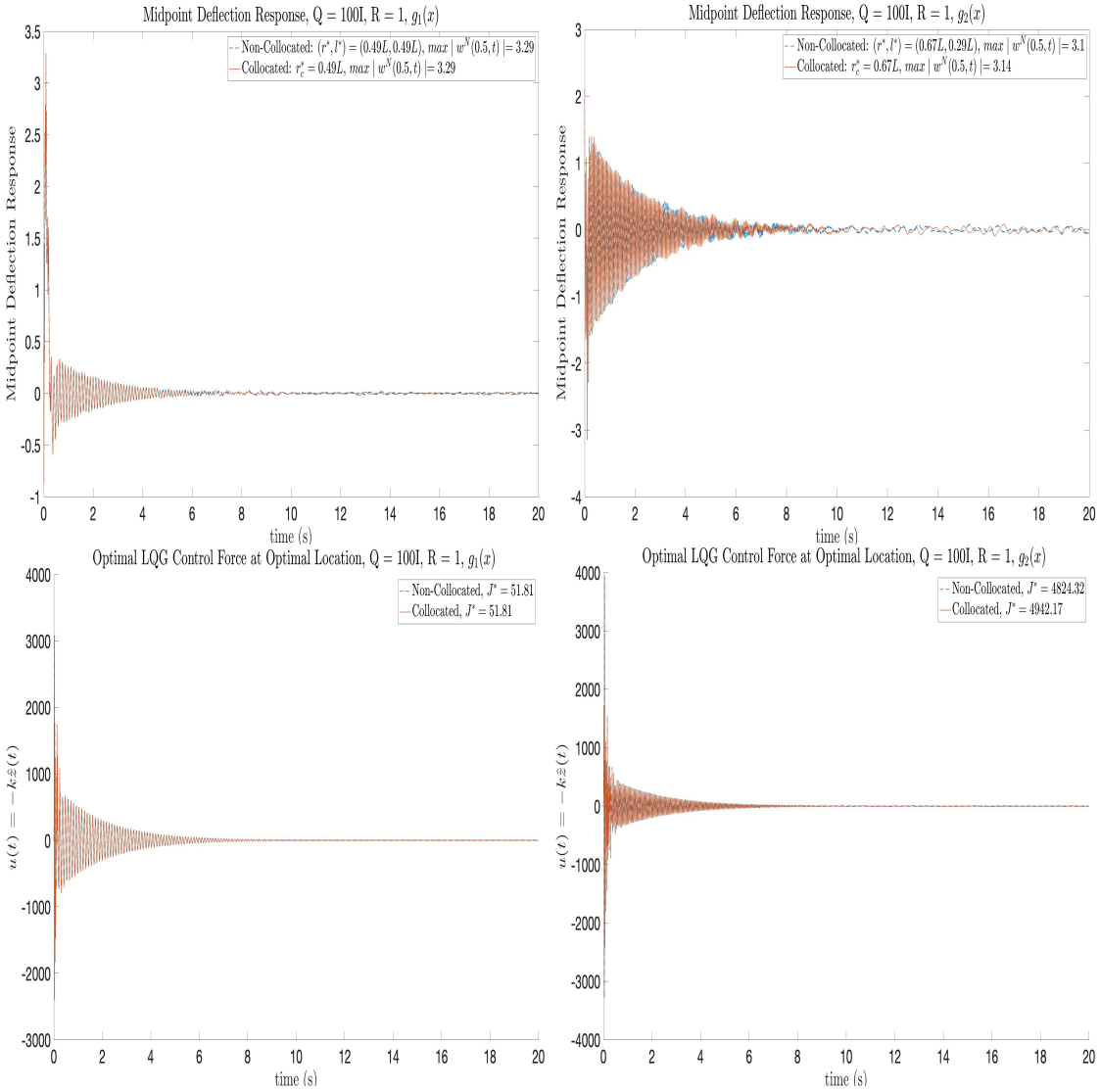

Figure 4.5: Compare performances of the non-collocated and collocated designs at their optimal locations.
Random initial condition z_{u_0} with 0 mean and unit variance.
Left: $Q = 100I$, uniform disturbance $g_1(x)$, $r^* = l^* = r_c^* = 0.49$ or 0.51.
$\frac{J^*(l^*,r^*) - J^*(r_c^*(1,1))}{J^*(r_c^*(1,1))} = 0\%$.
Right: $Q = 100I$, large peak disturbance $g_2(x)$, $r^* = 0.67$, $l^* = 0.29$, $r_c^* = 0.67$,
$\frac{J^*(l^*,r^*) - J^*(r_c^*(1,1))}{J^*(r_c^*(1,1))} = -2\%$ (units normalized by mass).

Chapter 5

Bridge Model Control

The bridge model has been developed to be a more realistic problem than the preliminary problem considered previously. The physical actuator dynamics is considered. The bridge system is subjected to more realistic disturbances instead of a white Gaussian disturbance. Thus, the $\mathbb{H}_2$ optimal controller is applied to aim at disturbance response controlling. It is compared to the mathematically equivalent LQG controller, with emphasis on the important differences in their motivations. A periodic pedestrian disturbance is considered. Actuator noise is added. A low pass filter for the low frequency walking disturbance is added to enhance control. The augmented plant that includes the non-Gaussian disturbances and weighting filter is constructed. In section 5.2, Example 5.2.2 and Example 5.2.3 illustrate the effectiveness of the augmented plant method and the effectiveness of the low pass filter.

In section 5.3, optimization is conducted to find the optimal locations for the non-collocated and collocated sensor/actuator designs, and comparisons of performances at the optimal locations of the two designs are presented.

5.1 Coupled Actuator-Structure Design

Interaction between the structure and controller devices may significantly affect the vibration dynamics. To include the interaction, the actuator of the controller is considered as a spring-mass damper system coupled to a fixed location on the bridge.

The work [24] has considered the interactions between an accelerometer sensor and a second order system as a coupled dynamical system, which are derived from the Hamilton's Principle. The work has a theorem (Theorem 6.1, [24]) that states:

If the second order system with state deflection $z(t)$ is coupled to the sensor and that $C_{l_{pos}} z(t)$ is the position of the structure where the sensor is attached, then the following equations describe the dynamics of the coupled system,

$$\begin{aligned} m\ddot{a}(t) + k(a(t) - C_{l_{pos}} z(t)) + d(\dot{a}(t) - C_{l_{pos}} \dot{z}(t)) = 0, \\ M\ddot{z}(t) + K_s z(t) + D\dot{z}(t) + kC^*_{l_{pos}}(C_{l_{pos}} z(t) - a(t)) + dC^*_{l_{pos}}(C_{l_{pos}} \dot{z}(t) - \dot{a}(t)) = B_{r_{pos}} u(t), \end{aligned} \tag{5.1.1}$$

where $a(t)$ is the deflection of the sensor, m, k, d are the sensor's mass, stiffness and damping parameters.

Assume that the actuator is fixed at an optimal location on the structure while applying the control force. The matrix $B_{r_{pos}}$ denotes the position of where the actuator is attached to the structure. The actuator deflection is a function of time only. The actuator is coupled with the Hermite basis FEM approximated time-dependent bridge dynamics in (2.2.10) using $N = 34$ number of elements, with the state variable $z_b^N(t) = [w_b^N(t), \dot{w}_b^N(t)]$. The number of elements is sufficient for the bridge structure state to converge to the modal approximated state. Their coupled motion of equations is derived via the Hamilton's Principle as in [24]. The control force $u(t)$ is directly applied to the actuator. Thus, $u(t)$ indirectly controls the bridge through the coupled actuator.

Let $a(t)$ denote the deflection of the actuator, m_a, k_a, d_a denote the actuator's mass, stiffness and damping parameters. Applying Theorem 6.1 in [24], the control force $u(t)$ is added to the actuator instead of to the structure by replacing the accelerator with an actuator and adding the modification. The force acting on the bridge by the actuator is $-B^N_{r_{pos}}(m_a\ddot{a})$, where

$$m_a\ddot{a}(t) = +d_a(B^{N^T}_{r_{pos}} \dot{w}_b^N(t) - \dot{a}(t)) + k_a(B^{N^T}_{r_{pos}} w_b^N(t) - a(t)) + u(t).$$

The coupled system of ODEs becomes

$$\begin{aligned} &M\ddot{w}_b^N(t) + D\dot{w}_b^N(t) + Kw_b^N(t) + k_a B_{r_{pos}}^N (B_{r_{pos}}^{N^T} w_b^N(t) - a(t)) + d_a B_{r_{pos}}^N (B_{r_{pos}}^{N^T} \dot{w}_b^N(t) - \dot{a}(t)) \\ &\quad = B_{1b}^N \omega_p(t) - B_{r_{pos}}^N \frac{u(t)}{m_a}, \\ &m_a \ddot{a}(t) + d_a(\dot{a}(t) - B_{r_{pos}}^{N^T} \dot{w}_b^N(t)) + k_a(a(t) - B_{r_{pos}}^{N^T} w_b^N(t)) \\ &\quad = u(t). \end{aligned} \tag{5.1.2}$$

Converting the coupled system (5.1.2) into state-space form by defining $z_p(t) \in \mathbb{R}^{2N+2q}$, where $q = 1$ is the single number of actuators, $z_p(t) = [w_b^N(t), \dot{w}_b^N(t), a(t), \dot{a}(t)]^T$.

From now, the superscript "N" on the approximated system will be dropped.

The coupled actuator-bridge plant dynamic system in the state-space form is

$$\begin{aligned} \dot{z}_p(t) &= A_p z_p(t) + B_{2p_r} u(t) + B_{1p}\omega_p(t),\ z_p(0) = z_{p0} = 0, \\ y_{2p} &= C_{2p_l} z_p + \nu(t), \end{aligned} \tag{5.1.3}$$

where $A_p = \begin{bmatrix} 0 & I & 0 & 0 \\ -[\frac{K + k_a B_{r_{pos}} B_{r_{pos}}{}^T}{M}] & -[\frac{D + d_a B_{r_{pos}} B_{r_{pos}}{}^T}{M}] & \frac{k_a}{M} B_{r_{pos}} & +\frac{d_a}{M} B_{r_{pos}} \\ 0 & 0 & 0 & I \\ \frac{k_a}{m_a} B_{r_{pos}}{}^T & \frac{d_a}{m_a} B_{r_{pos}}{}^T & -\frac{k_a}{m_a} & -\frac{d_a}{m_a} \end{bmatrix}$,

$$B_{2p_r} = \begin{bmatrix} 0 \\ -\frac{1}{m_a} B_{r_{pos}} \\ 0 \\ \frac{1}{m_a} \end{bmatrix}, B_{1p} = \begin{bmatrix} 0 \\ B_d^N \\ 0 \\ 0 \end{bmatrix}, C_{2p_l} = \begin{bmatrix} C_{l_{pos}}, 0, 0, 0 \end{bmatrix},$$

ω_p is the pedestrian disturbance defined in (5.2.9), and $\nu(t)$ is the sensor noise.

5.2 $\mathbb{H}_2$ Controller Design and the General Plant

For a realistic pedestrian disturbance, white Gaussian disturbance condition is not appropriate.

Closed-loop $\mathbb{H}_2$ control minimizes the norm of the disturbance response of a cost objective in the frequency domain. The cost objective is a combination of weighted state and weighted control. The $\mathbb{H}_2$ estimator minimizes the error of a linear combination of the estimated state and outputs the estimated linear combination of the state, usually in the form of the gain that leads to an output feedback controller. This is called the output estimator. The $\mathbb{H}_2$ output feedback finds the optimal control gain operator and connects to the $\mathbb{H}_2$ output estimator which provides the optimal estimated control using the gain operator. This closed-loop feedback system's realization in the time domain turns out to be mathematically equivalent to the LQG output feedback system. The $\mathbb{H}_2$ controller design in the time domain achieves the same minimal LQ performance index. However, the viewpoint is different from the LQG design, because the original $\mathbb{H}_2$ formulation in its frequency domain is motivated by controlling response to disturbances.

The derivations of $\mathbb{H}_2$ output feedback design from the frequency domain to the time domain can be found in textbooks such as [32] and [51], and will not be shown here. The following will discuss some important comparisons between these two controllers.

In both of the LQR and the $\mathbb{H}_2$ control designs, Π is the solution to the same ARE 3.1.9: $A^T\Pi + \Pi A + C_1^T C_1 - \Pi B_2 R_u^{-1} B_2^T \Pi = 0$. So the feedback control gain $K = R_u^{-1} B_2^T \Pi$ is the same. However, the objectives of the LQ performance index and $\mathbb{H}_2$ performance index are different. The LQ optimal control performance index is $J_{opt} = z_0^T \Pi z_0$, or for a random initial condition with covariance matrix Z_0, the optimal performance index is given by $J_{opt} = Tr(Z_0^{\frac{1}{2}} \Pi Z_0^{\frac{1}{2}})$. This implies that the objective of LQ control is to minimize the initial condition response. The $\mathbb{H}_2$ optimal control performance index is given by $J_{opt} = Tr(B_1^T \Pi B_1)$. This implies that the objective of the $\mathbb{H}_2$ control is to minimize the disturbance response.

Mathematically, both the Kalman and the optimal $\mathbb{H}_2$ estimators are exactly the same at minimizing the estimation error. In both designs, Σ is the solution to the same estimator associated ARE: $A\Sigma + \Sigma A^T + B_1 W B_1^T - \Sigma C_2^T R_e C_2 \Sigma = 0$. However, the estimators by themselves achieve different optimal cost values. The Kalman estimator provides minimum estimator error for the full state in the LQG controller, and achieves optimal value $\|\Sigma\|_1$. On the other hand, the $\mathbb{H}_2$ output estimator provides minimum estimator error for a selected linear combination of state to be used in the $\mathbb{H}_2$ control. The achieved optimal estimator value is influenced by control objective C_1: $< C_1, \Sigma C_1 >$. Details on output estimation can be found in the work [33] and in the textbook [32].

Consider the finite-dimensional system with control cost objective $y_1(t)$:

$$\begin{aligned} \dot{z}(t) &= Az(t) + B_2u(t) + B_1\omega_1(t),\ z(0) = z_0 = 0, \\ y_1(t) &= C_1z(t) + D_{12}u(t), \\ y_2(t) &= C_2z(t) + D_{21}\nu_1(t), \end{aligned} \tag{5.2.1}$$

where $z(t) \in \mathbb{R}^n$, $y_1(t) \in \mathbb{R}^j$, $y_2(t) \in \mathbb{R}^q$, $A \in \mathbb{R}^{n\times n}$, $B_2 \in \mathbb{R}^{n\times m}$, $B_1 \in \mathbb{R}^{n\times 1}$, $C_1 \in \mathbb{R}^{j\times n}$, $C_2 \in \mathbb{R}^{q\times n}$, $D_{21} \in \mathbb{R}^{j\times m}$, $D_{21} \in \mathbb{R}^{q\times m}$. The noises $\omega_1(t)$ and $\nu_1(t)$ are white Gaussian distributed. The integer, $n \in \mathbb{Z}$, denotes the number of states in the system, $j \in \mathbb{Z}$ denotes the number of independent costs considered in the control performance index, $m \in \mathbb{Z}$ denotes the number of actuators, and $q \in \mathbb{Z}$ denotes the number of sensors. In this thesis, $m = q = 1$.

Since the matrices and vectors are real matrices and vectors, matrix (vector) transpose is equivalent to the conjugate transpose "$*$" in the theorems. The matrices B_1, C_1 are finite-dimensional with finite-dimensional ranges, so they are automatically Hilbert-Schmidt operators and trace class. Details on operators in infinite-dimensional can be found in the textbook [32].

Define the following,
$A_c = A - B_2R^{-1}D_{12}^*C_1$, and $C_{1c} = (I - D_{12}R^{-1}D_{12}^*)C_1$,
$A_e = A - B_1D_{21}^*R_e^{-1}C_2$, and $B_{1e} = B_1(I - D_{21}^*R_e^{-1}D_{12})$.

Let $R_u = D_{12}^*D_{12} > 0$ and $R_e = D_{21}D_{21}^* > 0$ be coercive.

The $\mathbb{H}_2$ controller design is the design of an optimal $\mathbb{H}_2$ state estimator with an optimal $\mathbb{H}_2$ state feedback law.

Consider the following assumptions made for the controller and estimator:

Assumptions 1 *(H2 controller) (H1a)* $R_u = D_{12}^*D_{12}$ *is coercive.*
(H1b) $R_e = D_{21}D_{21}^*$ *is coercive.*
(H2a) (A, B_2) *is stabilizable.*
(H2b) (A, C_2) *is detectable.*

(H3a) (A_c, C_{1c}) *is detectable.*
(H3b) (A_e, B_{1e}) *is stabilizable.*

The following theorem for an infinite-dimensional system states the design of an optimal $\mathbb{H}_2$ output feedback controller, and is applied on the finite-dimensional system: (5.2.1).

Theorem 5.2.1 *($\mathbb{H}_2$ Output feedback design, Theorem 7.21 [32]) Consider the full-control system (5.2.1) and assume that in additional to the assumptions (H1)-(H3) at least one of the following holds:*

- B_1 *is a Hilbert-Schmidt operator,*
- C_1 *is a Hilbert-Schmidt operator,*
- *both* B_1 *and* C_1 *are trace class.*

Let $\Pi \in \mathcal{B}(\mathcal{Z}, \mathcal{Z})$, $\Pi dom(A) \subset dom(A^*)$ *be the positive semi-definite solution to*

$$(A_c^*\Pi + \Pi A_c - \Pi B_2 R_u^{-1} B_2^* \Pi + C_{1c}^* C_{1c})z = 0, \tag{5.2.2}$$

for all $z \in dom(A^*)$.

Let $\Sigma \in \mathcal{B}(\mathcal{Z}, \mathcal{Z})$, $\Sigma dom(A^*) \subset dom(A^*)$ *be the positive semi-definite solution to*

$$(\Sigma A_e^* + A_e \Sigma - \Sigma C_2^* R_e^{-1} C_2 \Sigma + B_{1e} B_{1e}^*)z = 0, \tag{5.2.3}$$

for all $z \in Dom(A^*)$.

The $\mathbb{H}_2$ *optimal state feedback gain is* $K = R_u^{-1} B_2^* \Pi + R_u^{-1} D_{12}^* C_1$ *and the filter is* $F = \Sigma C_2^* R_e^{-1} + B_1 D_{21}^* R_e^{-1}$. *The* $\mathbb{H}_2$ *controller* $z_e(t)$ *is*

$$\begin{aligned} z_e(t) &= (A - B_2 K - F C_2) z_e(t) + F y_2(t),\ z_e(0) = 0, \\ u(t) &= -K z_e(t). \end{aligned} \tag{5.2.4}$$

The optimal cost is
$\sqrt{trace(B_1^* \Pi B_1) + trace(R_e K \Sigma K^*)}$.

In order to apply the $\mathbb{H}_2$ control on the structural model with more realistic disturbances included, designing disturbance filters W_d, W_ν, W_η, and weight filter W_1 are required. The inclusion of various filters is called the augmented method, and the result coupled plant is known as the general plant or the augmented plant. The block diagram shown in Figure 5.1 in the frequency domain depicts a general plant.

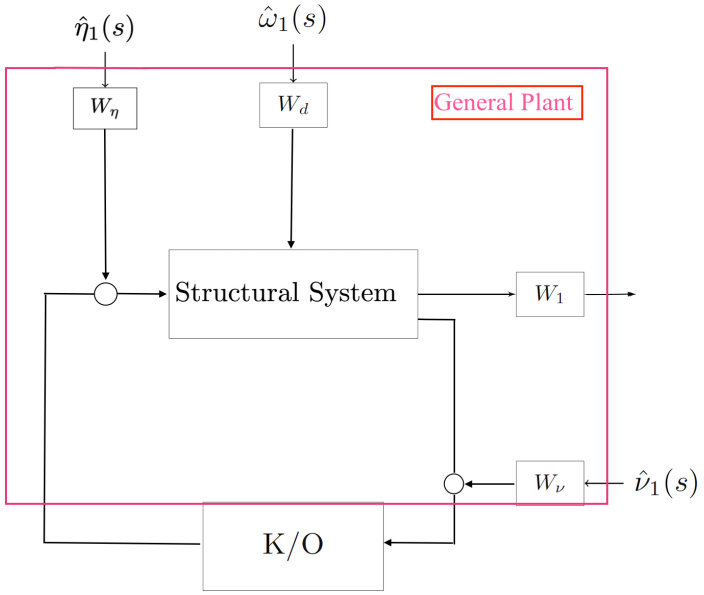

Figure 5.1: The $\mathbb{H}_2$ general plant in the frequency domain.

The general plant contains the actuator-coupled structural system, the weighting filter W_1, the disturbance filters W_d, W_ν and W_η that allow non-unit disturbances to be absorbed into the plant.

In the frequency domain, the non-uniform disturbance $\hat{\omega}_d(s)$ is shaped by a disturbance filter W_d, $\hat{\omega}_d(s) = W_d(s)\hat{\omega}_1(s)$, where $\hat{\omega}_1(s) = 1$ is uniform again. The disturbance filter W_d has an internal stable finite-dimensional realization $(A_{w_d}, B_{w_d}, C_{w_d}, 0)$, and the disturbance associated state in the time domain is $z_{w_d}(t)$. The following Example 5.2.2 and Figure 5.2 illustrate the efficiency of the augmented plant method over the simple non-augmented beam plant design in controlling the beam system in the preliminary problem (4.1.1) subject to a non-uniform disturbance.

Example 5.2.2 *Consider $z_u^N(t)$ and $(A_u^N, [B_{2u_r}^N, B_{1u}^N], C_{2u_l}^N)$ be the system from the preliminary problem (4.1.3), with fixed sensor actuator location at $l = r = 0.51$. Let $z_f(t)$ be the periodic load associated state with realization $(A_f, B_f, C_f, 0))$. $\omega_{per}(t) = e^{-0.0001} f sin(10.05t)$ can be rewritten in the form of $\omega_{per}(t) = C_f z_f(t)$. Let ω_1, ν_1 denote white Gaussian disturbances. Let $z_{aug}(t) = [z_b(t); z_f(t)]$ be the augmented state. The $\mathbb{H}_2$ control is applied to the augmented system*

$$\begin{aligned} \dot{z}_{aug}(t) &= A_{aug} z_{aug}(t) + B_{1_{aug}} \omega_1(t) + B_{2_{aug}} u(t),\ z_{aug}(0) = 0, \\ y_{1_{aug}}(t) &= C_{1_{aug}} z_{aug}(t) + 0.001 u(t), \\ y_{2_{aug}}(t) &= C_{2_{aug}} z_{aug}(t) + 0.002 \nu_1(t), \end{aligned} \tag{5.2.5}$$

where

$$A_{aug} = \begin{bmatrix} A_u & B_{1u} C_f \\ 0 & A_f \end{bmatrix}, B_{1_{aug}} = \begin{bmatrix} 0 \\ B_f \end{bmatrix}, B_{2_{aug}} = \begin{bmatrix} B_{2u_r} \\ 0 \end{bmatrix}, C_{2_{aug}} = \begin{bmatrix} C_{2u_l} & 0 \end{bmatrix}, C_{1_{aug}} = \begin{bmatrix} I & 0 \end{bmatrix}.$$

To compare with the non-augmented plant, the $\mathbb{H}_2$ control is applied to the non-augmented system

$$\begin{aligned} \dot{z}_u(t) &= A_u z_u(t) + B_{1u} \omega_{per}(t) + B_{2u_r} u(t),\ z_u(0) = 0, \\ y_{1u}(t) &= I z_u(t) + 0.001 u(t), \\ y_{2u}(t) &= C_{2u_l} z_u(t) + 0.002 \nu_1(t). \end{aligned} \tag{5.2.6}$$

The controlled responses and feedback $u(t)$ are shown in Figure 5.2. With much smaller controlled response and applied feedback control, the control performances on the augmented plant is better than that on the non-augmented simple beam plant. With the increase of disturbance intensity, i.e the increase of f, the benefit of incorporating disturbance into the system model becomes more prominent.

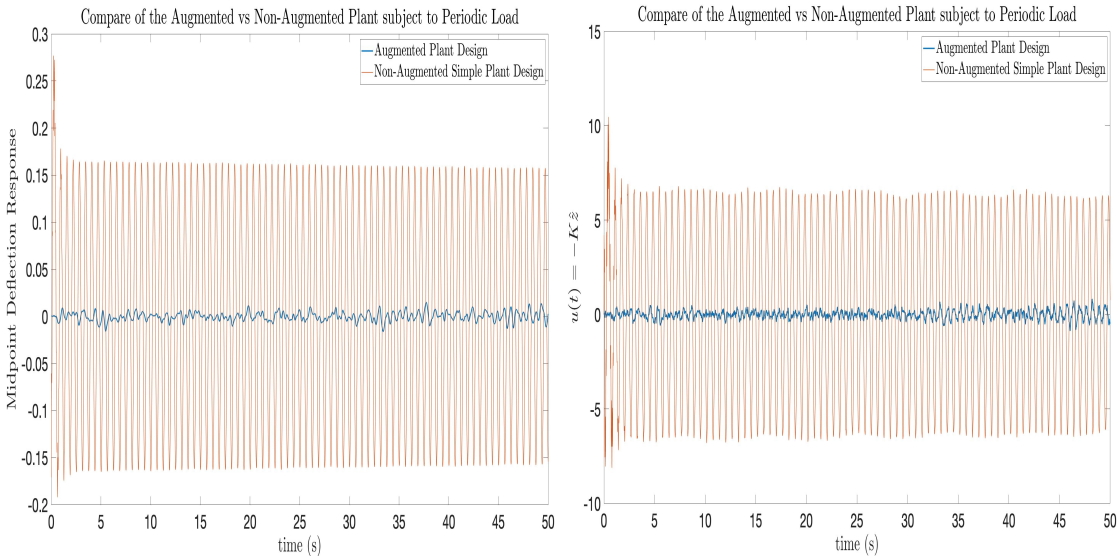

Figure 5.2: Ex.5.2.2: Compare periodic loading control performances on the augmented plant vs. simple non-augmented beam plant. Periodic load $\omega_{per}(t) = e^{-0.0001} f sin(10.05t)$, $f = 10$ (units normalized with respect to mass).

By inserting a low pass filter W_1 as part of the general plant, compared with not weighting on the lower frequencies, the controlled response is improved and the control force is much smaller. The following Example 5.2.3 and Figure 5.3 illustrate the efficiency of the low pass filter $\mathbb{H}_2$ control design over the non-filter $\mathbb{H}_2$ control design to control the beam system in the preliminary problem (4.1.1) subject to a white Gaussian disturbance.

Example 5.2.3 *Let $z_{Wl}(t)$ denote the low pass filter associated state with realization $(A_{Wl}, B_{Wl}, C_{Wl}, D_{Wl}) = (-20, 3\sqrt{20}, 100, 0)$ that weights the lower frequencies. The control objective is to reduce full state response to low frequency disturbance. The cost to be minimized is $y_1(t) = \begin{bmatrix} C_{Wl} z_u(t) \\ 0.0001 u(t) \end{bmatrix}$. Let $z_{lp}(t) = [z_u(t), z_{Wl}(t)]^T$ denote the $\mathbb{H}_2$ low pass filter augmented state. The $\mathbb{H}_2$ control is applied to the augmented system*

$$\begin{aligned} \dot{z}_{lp}(t) &= A_{lp} z_{lp}(t) + B_{1_{lp}} \omega_1(t) + B_{2_{lp}} u(t),\ z_{lp}(0) = 0, \\ y_{1_{lp}}(t) &= C_{1_{lp}} z_{lp}(t) + 0.001 u(t), \\ y_{2_{lp}}(t) &= C_{2_{lp}} z_{lp}(t) + 0.002 \nu_1(t), \end{aligned} \tag{5.2.7}$$

where $A_{lp} = \begin{bmatrix} A_u & 0 \\ B_{Wl} I & A_{Wl} \end{bmatrix}, B_{1_{lp}} = \begin{bmatrix} B_{1u} \\ 0 \end{bmatrix}, B_{2_{lp}} = \begin{bmatrix} B_{2u_r} \\ 0 \end{bmatrix}, C_{2_{lp}} = \begin{bmatrix} C_{2u_l} & 0 \end{bmatrix}, C_{1_{lp}} = \begin{bmatrix} 0 & C_{Wl} \end{bmatrix}.$

The $\mathbb{H}_2$ control is applied to the non-filter system

$$\begin{aligned} \dot{z_u}(t) &= A_u z_u(t) + B_{1u}\omega_1(t) + B_{2u_r}u(t),\ z_u(0) = 0, \\ y_{1u}(t) &= C_{Wl} z_u(t) + 0.001u(t), \\ y_{2u}(t) &= C_{2u_l} z_u(t) + 0.002\nu_1(t). \end{aligned} \tag{5.2.8}$$

The controlled responses and feedback $u(t)$ are shown in Figure 5.3. The low pass filter design controlled response performs better with a smaller amplitude, and the applied feedback control has a smaller amplitude than the non-filter design. The optimal performance index value of the low pass design is almost $\frac{1}{9}$ of the non-filter design's.

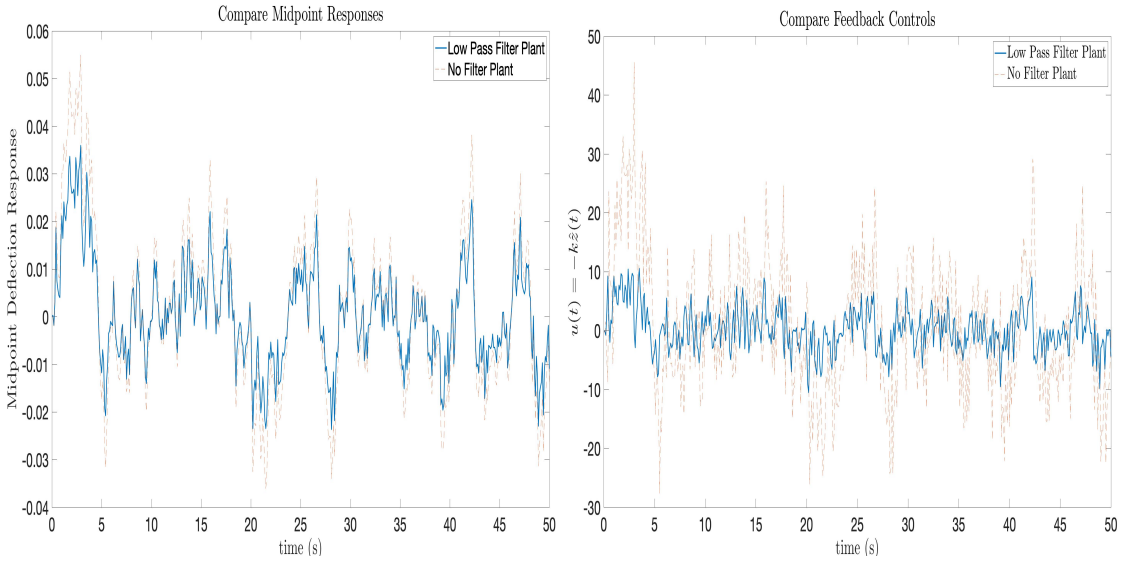

Figure 5.3: Ex.5.2.7: Compare $\mathbb{H}_2$ control performance of the low pass filter plant (with $\mathbb{H}_2$ optimal performance index: $J^* = 94$) and the non-filter plant (with $\mathbb{H}_2$ optimal performance index: $J^* = 843$) (units normalized with respect to mass).

In this thesis, the known input disturbance $\hat{\omega}_p(s)$ is shaped by W_p, i.e. $\hat{\omega}_p(s) = W_p(s)\hat{\omega}_1(s)$. Define its internal stable finite-dimensional realization to be $(A_W, B_W, C_W, 0)$, and the shaped disturbance state to be $z_{d_p}(t)$. To satisfy the $\mathbb{H}_2$ control assumptions on (H2a) and (H3b), a little amount of damping, ζ_{ped}, on the pedestrian load in (2.1.8) is added,

$$\omega_p(t) = -e^{-\zeta_{ped}t}W_{ped} - 0.37e^{-\zeta_{ped}t}W_{ped}\sin(2\pi f_s t). \tag{5.2.9}$$

This yields a coupled first order and second order realizations, with $z_{d_p}(t) \in \mathbb{R}^3$:

$$A_W = \begin{bmatrix} -\zeta_{ped} & 0 & 0 \\ 0 & 0 & 1 \\ 0 & -(f_s^2 + \zeta_{ped}^2) & -2\zeta_{ped} \end{bmatrix}, B_W = \begin{bmatrix} 1 \\ 0 \\ 1 \end{bmatrix}, C_W = -W_{ped} \begin{bmatrix} 1 & 0.37 f_s & 0 \end{bmatrix}.$$

Actuator device noises are considered. In this thesis, the actuator device noises is shaped by $W_\eta(s) = 0.1 + \frac{0.01}{s+100}$ such that it is present at all frequencies. Let $\eta(s) = W_\eta(s)\hat{\eta_1}(s)$, where $\hat{\eta_1}(s)$ is uniform disturbance. Define its internal stable finite-dimensional realization to be $(A_\eta, B_\eta, C_\eta, D_\eta)$, and the shaped disturbance state to be $z_\eta(t)$.

Sensor device noises are usually assumed to be Gaussian noises. Thus, the sensor noise in this thesis will be considered as a Gaussian noise with variance $\delta_n \in \mathbb{R}$. Hence, the sensor noise filter W_ν in Figure 5.1 is not needed.

The pedestrian disturbance is in the lower frequency range, so the controller should aim at minimizing disturbance response for the lower frequency range. Thus, a low pass frequency disturbance weighting in the controller design objective is applied. The dominant walking frequency is considered as 1.6 Hz in this thesis, so $W_1(s)$ will be a first order weighting transfer function that weights heavily on the lower frequencies for state responses and drops dramatically after 1.6 Hz. Denote the stable finite-dimensional realization of the transfer function from $Q_0^{\frac{1}{2}}\hat{z}_p(s)$ to the cost, $W_1\hat{z}_{W_1}(s)$, to be $(A_{W_1}, B_{W_1}, C_{W_1}, 0)$. Let $z_{W_1}(t) \in \mathbb{R}^1$ denote the state weighted by W_1. The control goal is to minimize the response of a weighted plant state $Q_0^{\frac{1}{2}}\hat{z}_p(s)$ to low frequency disturbance. Let $\delta_u << 1$ denote the control weight such that the control is nonsingular.

The total cost for the augmented system in the time domain is

$$y_1(t) = C_{W_1} z_{W_1}(t) + \delta_u u(t). \tag{5.2.10}$$

Define the augmented state for the general plant $z_{au}(t) = [z_p(t), z_{W_1}(t), z_{d_p}(t), z_\eta(t)]^T$, and all the uniform Gaussian disturbances $d(t) = [\omega_1(t), \nu_1(t), \eta_1(t)]^T$. The augmented

system of equations becomes

$$\begin{aligned}
\dot{z}_p(t) &= A_p z_p(t) + B_{2p_r} u(t) + B_{2p_r}\eta(t) + B_{1p}\omega_p(t),\\
y_{2p}(t) &= C_{2p_l} z_p(t) + \delta_n \nu_1(t),\\
\dot{z_{W_1}}(t) &= A_{W_1} z_{W_1}(t) + B_{W_1} Q_0^{\frac{1}{2}} z_p(t),\\
y_1(t) &= C_{W_1} z_{W_1}(t) + \delta_u u(t),\\
\dot{z}_{d_p}(t) &= A_w z_{dp}(t) + B_w \omega_1(t),\\
\omega_p(t) &= C_w z_{d_p}(t),\\
\dot{z_\eta}(t) &= A_\eta z_\eta(t) + B_\eta \eta_1(t),\\
\eta(t) &= C_\eta z_\eta(t) + D_\eta \eta_1(t).
\end{aligned}$$

Define the matrices:

$$A_r = \begin{bmatrix} A_p & 0 & B_{1p}C_w & B_{2p_r}C_\eta \\ B_{W_1}Q_0^{\frac{1}{2}} & A_{W_1} & 0 & 0 \\ 0 & 0 & A_w & 0 \\ 0 & 0 & 0 & A_\eta \end{bmatrix},$$

$$B_{1r} = \begin{bmatrix} B_{1p}D_w & 0 & B_{2p_r}D_\eta \\ 0 & 0 & 0 \\ B_w & 0 & 0 \\ 0 & 0 & B_\eta \end{bmatrix}, B_{2r} = \begin{bmatrix} B_{2p_r} \\ 0 \\ 0 \\ 0 \end{bmatrix},$$

$$C_1 = \begin{bmatrix} 0 & C_{W_1} & 0 & 0 \\ 0 & 0 & 0 & 0 \end{bmatrix}, C_{2l} = \begin{bmatrix} C_{2p_l} & 0 & 0 & 0 \end{bmatrix},$$

$$D_{12} = \begin{bmatrix} 0 \\ \delta_u \end{bmatrix}, D_{21} = \begin{bmatrix} 0 & \delta_n & 0 \end{bmatrix}.$$

The state-space form of the augmented plant is

$$\begin{aligned}
\dot{z}_{au}(t) &= A_r z_{au}(t) + B_{2r} u(t) + B_{1r} d(t),\ z_{au}(0) = z_0 = 0,\\
y_1(t) &= C_1 z_{au}(t) + D_{12} u(t),\\
y_2(t) &= C_{2l} z_{au}(t) + D_{21} d(t).
\end{aligned} \tag{5.2.11}$$

The optimal $\mathbb{H}_2$ performance index of this system is

$$J(z_{au}, u) = \int_0^\infty \|C_1 z_{au} + D_{21} u\|_2^2 \, dt. \tag{5.2.12}$$

This augmented system is in the form of (5.2.1), with $A = A_r$, $B_1 = B_{1r}$, $B_2 = B_{2r}$, $C_1 = C_1$, $C_2 = C_{2l}$, $D_{12} = D_{12}$, $D_{21} = D_{21}$, $\omega_1 = d(t)$. The actuator location r dependent matrices are A_r, B_{1r}, B_{2r} and the sensor location l dependent matrix is C_{2l}.

The augmented system satisfies the assumptions in Theorem 5.2.1, and orthogonality holds, $D_{12}^T C_1 = 0$ and $B_{1r} D_{21}^T = 0$. Thus, $A_c = A_r$, $A_e = A_r$, $C_{1c} = C_1$ and $B_{1e} = B_{1r}$ in Theorem 5.2.1. The $\mathbb{H}_2$ controller is

$$\begin{aligned} z_e(t) &= (A_r - B_{2r}K(r) - F(l)C_{2l})z_e(t) + F(l)y_{2_l}(t), \; z_e(0) = 0, \\ u^*(t) &= -K(r)z_e(t), \end{aligned} \tag{5.2.13}$$

where $K(r) = R_u^{-1} {B_{2r}}^T \Pi(r)$, and $\Pi(r)$ is the solution to the actuator location-parameterized ARE

$$A_r^T \Pi(r) + \Pi(r) A_r - \Pi(r) B_{2r} R_u^{-1} B_{2r}^T \Pi(r) + C_1^T C_1 = 0, \tag{5.2.14}$$

$F(l, r) = \Sigma(l, r) {C_{2l}}^T R_e^{-1}$, and $\Sigma(l, r)$ is the solution to the sensor/actuator location-parameterized ARE

$$\Sigma(l, r) A_r^T + A_r \Sigma(l, r) - \Sigma(l, r) C_{2l}^T R_e^{-1} C_{2l} \Sigma + B_{1r} B_{1r}^T = 0, \tag{5.2.15}$$

and the optimal cost is

$$\sqrt{Tr(B_{1r}^T \Pi(r) B_{1r}) + Tr(R_e K(r) \Sigma(l, r) K(r)^T)}.$$

This problem is interesting since the estimator associated ARE relies on both the sensor and actuator locations. In the preliminary problem and other works found in the literature review, the estimator design solely relies on the measurement location, and the control design solely relies on the actuator location. However, by modelling the actuator noise in the system, it makes sense that the design of the estimator is now affected by the actuator location.

Define the location optimization cost functional to be the squared optimal $\mathbb{H}_2$ performance index

$$J^*(l,r) := Tr(B_{1r}^T \Pi(r) B_{1r}) + Tr(R_e K(r) \Sigma(l,r) K(r)^T). \tag{5.2.16}$$

The optimization problem defined for the non-collocated sensor/actuator design (4.1.13) and the collocated sensor/actuator design (4.1.15) with $J^*(l,r)$ defined in (5.2.16) are applied to find the optimal non-collocated sensor/actuator locations (l^*, r^*) defined in (4.1.14) and the optimal collocated sensor/actuator locations r_c^* defined in (4.1.16).

5.3 Simulation Results of the Location Optimization Problem on the Bridge

The parameters of the bridge are referenced from [16], using consistent mass matrix that assumes uniformly distributed mass on the element. The parameters of the bridge-actuator system are given in Table 5.1, the parameters of the pedestrian disturbance are given in Table 5.2, and the filters' realization are given in Table 5.3.

Three state weights on the plant state $z_p(t)$ that result in different scales of the location optimization cost functional are considered in the simulations. As seen in the preliminary results, the scale of the location optimization cost functional range is associated with the optimal locations and the differences in the performance of the non-collocated sensor/actuator and collocated sensor/actuator controllers at their optimal locations. The state weight matrix Q_0 on the plant state $z_p(t)$ is defined by

$$Q_0 z_p(t) = \begin{bmatrix} \beta_p EI K^I & 0 & 0 & 0 \\ 0 & \beta_k \rho M^I & 0 & 0 \\ 0 & 0 & \lambda_{K^I} \beta_p EI & 0 \\ 0 & 0 & 0 & \lambda_{M^I} \beta_k \rho \end{bmatrix} z_p(t), \tag{5.3.1}$$

where K^I,M^I are the state energy weighting matrices derived in (3.3.14) with $C_{1_1} = \beta_p EI$ and $C_{1_2} = \beta_k \rho$ being the potential and kinetic energy weights. The actuator state is weighted proportional to the maximum eigenvalues of the potential and kinetic energy state weight matrices denoted by λ_{K^I} and λ_{M^I}. Define the notation $(\beta_p, \beta_k)_I$ to indicate the state weight Q_0 weighing $\beta_p EI$ on the potential energy and weighing $\beta_k \rho$ on the kinetic energy. The three state weights used in the Matlab simulations are given in Table 5.4.

Define Ω_l, $\Omega_r = X_1 : 0.92\Delta : X_2$ in Matlab, where X_1, X_2 are the spatial nodal coordinates of the first and last free node of the finite element nodes. The possible sensor/actuator locations are evenly spaced 0.92 of the sensor/actuator width Δ apart.

Table 5.1: Bridge-Actuator System Parameter Values

Symbol	Descriptive Name	Value
L	Bridge Length (m)	16.76
M	Bridge Mass (kg)	1800
E	Young's Modulus (GPa)	69
I	Moment of Inertia (m^4)	50×10^{-6}
ζ	Damping ratio	1% (Fundamental Mode)
Δ	Actuator/Sensor Width (m)	0.02L
m_a	Actuator Mass (kg)	0.07M
k_a	Actuator Stiffness (N/m)	$9.81m_a$
d_a	Actuator Damping (Ns/m)	$2\sqrt{ka/ma}0.9$
δ_ν	Sensor Noise	0.002
δ_u	Control Weight	0.001

Table 5.2: Pedestrians Disturbance Parameter Values

Symbol	Descriptive Name	Value
W_{ped}	Pedestrian Weight (N)	70×9.81
n_{ped}	Number of Pedestrians	3
f_s	Fundamental Pacing Frequency (Hz)	1.6
η_p^1	Fundamental Periodic Loading Factor	0.37
ζ_{ped}	Loading Damping Factor	0.0001
$g_p(x)$	Disturbance Spatial Distribution	$g_p(x) = n_{ped}/L$

Table 5.3: First Order Filter Realizations

State	Descriptive Name	Realization (A_i, B_i, C_i, D_i)
z_{W_1}	Low Pass Filter	$(-2\pi f_s, \sqrt{2\pi f_s}, 100\sqrt{2\pi f_s}, 0)$
z_η	Actuator Noise	$(-100, 0.01, 1, 0.1)$

Table 5.4: State Weight Q_0 Cases

case #	Descriptive Name	$(\beta_p c_1, \beta_k c_2)$	Notation: (β_p, β_k)
1	Large Scale Weight	$(20EI, 0.0001\rho)$	$(20, 0.0001)_I$
2	Intermediate Scale Weight	(EI, ρ)	$(1, 1)_I$
3	Small Scale Weight	$(0.0001EI, 0.01\rho)$	$(0.0001, 0.01_I)$

Let (l, r) denote a pair of sensor/actuator locations; (l^*, r^*) denote the non-collocated sensor/actuator controller's optimal sensor location and optimal actuator location correspondingly, and r_c^* denotes the optimal collocated sensor/actuator location.

The performances of the controllers are defined by the bridge's controlled deflection and velocity responses and the controller's feedback force. A human's perception of a stable surface is associated with the velocity of the system [43]. Therefore, this chapter focuses on comparing the velocity responses.

Define the relative controlled deflection norms, velocity response norms and feedback control norms at one location (l_1, r_1) to another location (l_2, r_2) as

$$\begin{aligned} w_{rel} &:= \frac{\left\|w(0.5)_{(l_1,r_1)}\right\|_{\mathcal{L}_2} - \left\|w(0.5)_{(l_2,r_2)}\right\|_{\mathcal{L}_2}}{\left\|w(0.5)_{(l_2,r_2)}\right\|_{\mathcal{L}_2}}, \\ v_{rel} &:= \frac{\left\|v(0.5)_{(l_1,r_1)}\right\|_{\mathcal{L}_2} - \left\|v(0.5)_{(l_2,r_2)}\right\|_{=\mathcal{L}_2}}{\left\|v(0.5)_{(l_2,r_2)}\right\|_{\mathcal{L}_2}}, \\ u_{rel} &:= \frac{\left\|u(0.5)_{(l_1,r_1)}\right\|_{\mathcal{L}_2} - \left\|u(0.5)_{(l_2,r_2)}\right\|_{\mathcal{L}_2}}{\left\|u(0.5)_{(l_2,r_2)}\right\|_{\mathcal{L}_2}}. \end{aligned} \tag{5.3.2}$$

Since physical systems and devices have limitations in their tolerance to force and exertion of force, it is reasonable to compare the relative maximum responses of the bridge

and the maximum feedback control. Define the relative maximum controlled deflection and velocity responses and maximum feedback control at one location (l_1, r_1) to another location (l_2, r_2) as

$$\begin{aligned} w_{rel}^{\infty} &:= \frac{\left\|w(0.5)_{(l_1,r_1)}\right\|_{\infty} - \left\|w(0.5)_{(l_2,r_2)}\right\|_{\infty}}{\left\|w(0.5)_{(l_2,r_2)}\right\|_{\infty}}, \\ v_{rel}^{\infty} &:= \frac{\left\|v(0.5)_{(l_1,r_1)}\right\|_{\infty} - \left\|v(0.5)_{(l_2,r_2)}\right\|_{\infty}}{\left\|v(0.5)_{(l_2,r_2)}\right\|_{\infty}}, \\ u_{rel}^{\infty} &:= \frac{\left\|u_{(l_1,r_1)}\right\|_{\infty} - \left\|u_{(l_2,r_2)}\right\|_{\infty}}{\left\|u_{(l_2,r_2)}\right\|_{\infty}}. \end{aligned} \tag{5.3.3}$$

The more negative the relative performances are, the better the performances of the non-collocated sensor/actuator design are.

Details of the results for each case are presented in the rest of this section.

Table 5.5 on the next page shows the relative changes in performance index at the optimal locations of the non-collocated to the collocated sensor/actuator design, defined as J_{rel}^{*} in the below equation (5.3.4), and the optimal locations of the non-collocated and the collocated sensor/actuator from simulations using the three state weights. The order presented is from the largest scale of the location optimization cost functional range to the smallest scale.

Define the relative changes in performance index at the optimal locations of the non-collocated to the collocated sensor/actuator design as

$$J_{rel}^{**} := \frac{J_{N.C.}^{*} - J_{Col}^{*}}{J_{Col}^{*}}, \tag{5.3.4}$$

where $J_{N.C.}^{*} = J^{*}(l^{*}, r^{*})$, $J_{Col}^{*} = J^{*}(r_c^{*})$.

Table 5.5: Compare relative optimal performance index at the optimal location and optimal locations for the three state weight cases; l^*: the optimal non-collocated sensor location, r^* : the optimal actuator location, r_c^*: the optimal collocated sensor/actuator location, values inside brackets denote the corresponding symmetric optimal locations; $J_{N.C.}^* = J^*(l^*, r^*)$: optimal performance index at the non-collocated optimal location (l^*, r^*); $J_{Col}^* = J^*(r_c^*)$: the optimal performance index at the collocated sensor/actuator optimal location r_c^*; $J_{rel}^\star := \frac{J_{N.C.}^* - J_{Col}^*}{J_{Col}^*}$.

(β_p, β_k)	$J^*(l^*, r^*)$	J_{rel}^{**}	l^*	$r^* = r_c^*$
$(20, 0.0001)_I$	1.13×10^{12}	-0.00002%	$0.872L(0.128L)$	$0.502L(0.498L)$
$(1, 1)_I$	5.67×10^{10}	-0.98%	$0.354L(0.646L)$	$0.502L$
$(0.001, 0.01)_I$	5.79×10^{7}	-2.00%	$0.631L(0.369L)$	$0.502L$

Table 5.6 on next page shows the comparisons on the performances of the optimally located non-collocated sensor/actuator controller to the optimally located collocated sensor/actuator controller, to the non-optimal randomly located sensor/actuator controller with actuator at r^*, and to the non-optimal collocated sensor/actuator controller at l^*.

Table 5.6: Relative controlled response $\mathcal{L}_2$-norms and control feedback $\mathcal{L}_2$-norms of the optimally located non-collocated sensor/actuator controller to:
the collocated sensor/actuator designed controller,
the non-optimal randomly located sensor/actuator controller with actuator at r^*,
and to the non-optimal located collocated sensor/actuator controller at l^*.
$J^*_{N.C.} = J^*(l^*, r^*)$: optimal performance index at the non-collocated optimal location (l^*, r^*),
$J^*_2 = J^*(l_2, r_2)$: optimal performance index at the location (l_2, r_2),
$J^*_{rel} := \frac{J^*_{N.C.} - J^*_2}{J^*_2}$.
Relative response norms at a location (l_1, r_1) to another location (l_2, r_2):
$w_{rel} := \frac{\left\|w(0.5)_{(l_1,r_1)}\right\|_{\mathcal{L}_2} - \left\|w(0.5)_{(l_2,r_2)}\right\|_{\mathcal{L}_2}}{\left\|w(0.5)_{(l_2,r_2)}\right\|_{\mathcal{L}_2}}$,
$v_{rel} := \frac{\left\|v(0.5)_{(l_1,r_1)}\right\|_{\mathcal{L}_2} - \left\|v(0.5)_{(l_2,r_2)}\right\|_{=\mathcal{L}_2}}{\left\|v(0.5)_{(l_2,r_2)}\right\|_{\mathcal{L}_2}}$,
$u_{rel} := \frac{\left\|u(0.5)_{(l_1,r_1)}\right\|_{\mathcal{L}_2} - \left\|u(0.5)_{(l_2,r_2)}\right\|_{\mathcal{L}_2}}{\left\|u(0.5)_{(l_2,r_2)}\right\|_{\mathcal{L}_2}}$.

Case/ Locations	J^*_{rel}	w_{rel}	v_{rel}	u_{rel}
$(20, 0.0001)_I$				
(l^*, r^*) vs. r^*_c	0%	−1.92%	0.43%	0.22%
(l^*, r^*) vs.Non-optimal$(0.24L, r^*)$	0%	−2.97%	0.51%	0.43%
(l^*, r^*) vs.Non-optimal(l^*, l^*)	−89.70%	−75.54%	−58.83%	−46.94%
$(1, 1)_I$				
(l^*, r^*) vs. r^*_c	−0.98%	−12.05%	−1.45%	0.68%
(l^*, r^*) vs.Non-optimal$(0.33L, r^*)$	−10.56%	−50.3%	−18.94%	4.81%
(l^*, r^*) vs.Non-optimal(l^*, l^*)	−58.78%	86.95%	−29.36%	−8.14%
$(0.001, 0.01)_I$				
(l^*, r^*) vs. r^*_c	−2%	−10.79%	3.33%	0.71%
(l^*, r^*) vs.Non-optimal$(0.24L, r^*)$	−1.34%	−17.77%	3.62%	1.06%
(l^*, r^*) vs.Non-optimal(l^*, l^*)	−54.11%	−64.59%	−58.86%	−7.07%

Table 5.7: Relative maximum controlled responses and control feedback of the optimally located non-collocated sensor/actuator controller to:
the collocated sensor/actuator designed controller,
the non-optimal randomly located sensor/actuator controller with actuator at r^*,
and to the non-optimal located collocated sensor/actuator controller at l^*.
$J^*_{N.C.} = J^*(l^*, r^*)$: optimal performance index at the non-collocated optimal location (l^*, r^*),
$J^*_2 = J^*(l_2, r_2)$: optimal performance index at the location (l_2, r_2),
$J^*_{rel} := \frac{J^*_{N.C.} - J^*_2}{J^*_2}$. Relative maximum responses at a location (l_1, r_1) to another location (l_2, r_2):
$w^\infty_{rel} := \frac{\left\|w(0.5)_{(l_1,r_1)}\right\|_\infty - \left\|w(0.5)_{(l_2,r_2)}\right\|_\infty}{\left\|w(0.5)_{(l_2,r_2)}\right\|_\infty}$,
$v^\infty_{rel} := \frac{\left\|v(0.5)_{(l_1,r_1)}\right\|_\infty - \left\|v(0.5)_{(l_2,r_2)}\right\|_\infty}{\left\|v(0.5)_{(l_2,r_2)}\right\|_\infty}$,
$u^\infty_{rel} := \frac{\left\|u_{(l_1,r_1)}\right\|_\infty - \left\|u_{(l_2,r_2)}\right\|_\infty}{\left\|u_{(l_2,r_2)}\right\|_\infty}$.

Case/ Locations	J^*_{rel}	w^∞_{rel}	v^∞_{rel}	u^∞_{rel}
$(20, 0.0001)_I$				
(l^*, r^*) vs. r^*_c	0%	−1.84%	0%	−1.83%
(l^*, r^*) vs.Non-optimal$(0.24L, r^*)$	0%	−3.61%	0%	0%
(l^*, r^*) vs.Non-optimal(l^*, l^*)	−89.70%	−71.87%	−63.59%	−33.86%
$(1, 1)_I$				
(l^*, r^*) vs. r^*_c	−0.98%	−10.38%	1.37%	1.38%
(l^*, r^*) vs.Non-optimal$(0.33L, r^*)$	−10.56%	−39.69%	−22.11%	13.46%
(l^*, r^*) vs.Non-optimal(l^*, l^*)	−58.78%	71.17%	−33.93%	−2.49%
$(0.001, 0.01)_I$				
(l^*, r^*) vs. r^*_c	−2%	−6.25%	2.6%	2.67
(l^*, r^*) vs.Non-optimal$(0.24L, r^*)$	−1.34%	−7.41%	−0%	5.92%
(l^*, r^*) vs.Non-optimal(l^*, l^*)	−54.11%	−62.06%	−60.00%	0.61%

Table 5.8: Relative error in estimations at the optimally located non-collocated sensor/actuator controller (l^*, r^*),
the optimally located collocated sensor/actuator controller (r_c^*, r_c^*),
the non-optimal randomly located sensor/actuator controller at (l, r^*),
and the non-optimal located collocated sensor/actuator controller at (l^*, l^*).
$e_w^{\mathcal{L}_2} := \frac{\|w_e - w\|_2}{\|w\|_2}$, $e_v^{\mathcal{L}_2} := \frac{\|v_e - v\|_2}{\|v\|_2}$, where w_e and v_e are the estimated deflection and velocity.

Case/ Locations	$error_w^{\mathcal{L}_2}$	$error_v^{\mathcal{L}_2}$
$(20, 0.0001)_I$		
(l^*, r^*)	0.0021	0.0090
(r_c^*, r_c^*)	0.0024	0.0334
Non-optimal $(0.24L, r^*)$	0.005	0.0586
Non-optimal (l^*, l^*)	0.0013	0.0082
$(1, 1)_I$		
(l^*, r^*)	0.0083	0.1227
(r_c^*, r_c^*)	0.0036	0.0419
Non-optimal $(0.33L, r^*)$	0.0165	0.3805
Non-optimal (l^*, l^*)	0.0130	0.0349
$(0.001, 0.01)_I$		
(l^*, r^*)	0.0050	0.0439
(r_c^*, r_c^*)	0.0037	0.0408
Non-optimal $(0.24L, r^*)$	0.0072	0.0716
Non-optimal (l^*, l^*)	0.0026	0.0170

For case 1, the scale of the overall performance index is relatively large. The performance with respect to the actuator locations resembles a steep concave up shape relationship, and the minima are near the center. The performance with respect to the sensor locations resembles a constant relationship. The optimal locations of the non-collocated and collocated actuator are the same at 50.2% of the bridge length. The non-collocated sensor optimal locations are far away from the centers, at $0.13L$ and $0.87L$ on the bridge. The controlled responses and feedback controls of the two controllers are almost identical. The relative difference in the deflection $\mathcal{L}_2$-norms of the two designs is less than 2%, the relative difference in the velocity and feedback $\mathcal{L}_2$-norms are less than 0.5%. The relative errors in estimating deflection response and velocity response are smaller in the non-collocated sensor/actuator design at its optimal locations than the collocated sensor/actuator design at its optimal locations, but not smaller than the collocated sensor/actuator design at the non-collocated sensor optimal location l^*. (See Figure 5.4 for performance index vs. sensor actuator locations and Figure 5.5 for performances of the non-collocated sensor/actuator and collocated sensor/actuator controllers).

For case 2, the scale of the overall performance index is intermediate among the three cases. The performance with respect to the actuator locations resembles a flatter concave up shape relationship compared with case 1. The performance with respect to the sensor locations is almost constant. The optimal locations of the non-collocated and collocated actuator are the same at 50.2% of the bridge length. The non-collocated sensor optimal locations moves closer toward to centers compare to in case 1. The relative difference in the deflection $\mathcal{L}_2$-norms of the two designs is 12.05%, and the relative difference in the velocity and feedback $\mathcal{L}_2$-norms are less than 2%. The relative errors in estimating deflection response and velocity response are larger in the non-collocated sensor/actuator design at its optimal locations than the collocated sensor/actuator design at its optimal locations and at the non-collocated sensor optimal location l^*. (See figure 5.6 for performance index vs. sensor actuator locations and figure 5.7 for performances of the non-collocated sensor/actuator and collocated sensor/actuator controllers).

For case 3, the scale of the overall performance index is the smallest among the three cases. The performance with respect to the locations becomes a flatter concave up shape relationship compared with cases 1 and 2. The performance with respect to the sensor locations is almost constant. The optimal locations of the non-collocated and collocated actuator are the same at 50.2% of the bridge length. The non-collocated sensor optimal locations are closer to the centers than in cases 1 and 2. The relative difference in the deflection $\mathcal{L}_2$-norms of the two designs is 10.79%, the relative difference in the velocity and

feedback $\mathcal{L}_2$-norms are less than 3%. The relative errors in estimating deflection response and velocity response are larger in the non-collocated sensor/actuator design at its optimal locations than the collocated sensor/actuator design at its optimal locations and at the non-collocated sensor optimal location l^*. (See figure 5.8 for performance index vs. sensor actuator locations and figure 5.9 for performances of the non-collocated sensor/actuator and collocated sensor/actuator controllers).

The main goal of this thesis is to study the differences in the optimally located non-collocated sensor/actuator and the optimally located collocated sensor/actuator controllers' performances. The results show that the optimal locations of the actuators of the two designs are the same, with $r^* = r_c^*$. The potential differences in the two designs' performances are caused by the optimal non-collocated sensor locations. Actuator position seems to dominate the performance index values over the sensor locations especially when the scale of the location optimization cost functional range is large. The non-collocated sensor/actuator controllers fixed at the optimal actuator locations with various non-optimal sensor locations performs similar to the optimally located controller.

In all cases, the optimal locations of the actuators for both designs are the same, with $r^* = r_c^*$ being almost at the bridge's center, and the optimal locations of the non-collocated sensor are causing the performance difference in the two designs. The optimal locations of the non-collocated sensor, l^*, change in different cases. The different sensor optimal locations consequently lead to the differences in the non-collocated sensor/actuator and the collocated sensor/actuator controllers. Thus, the state weight impacts the differences in performances of the non-collocated sensor/actuator and collocated sensor/actuator controllers at their optimal locations. See Table 5.5 for the optimal locations of the two controllers.

Although the non-collocated sensor/actuator design usually yields the smallest performance index, its optimal performance index is only relatively smaller to the collocated sensor/actuator performance index by at most 2%. The controlled responses are almost identical, with the non-collocated sensor/actuator controller yielding a relatively smaller $\mathcal{L}_2$-norm of deflection response by at most 12% and a relatively smaller $\mathcal{L}_2$-norm of velocity response by at most 2%. See Table 5.6. The non-collocated sensor/actuator controller yields a relatively smaller maximum amplitude of the deflection response by at most 11%, but a larger maximum amplitude of the velocity response by almost 3%. This implies that the collocated sensor/actuator design at its optimal location is only slightly higher in performance index and can be better in controlling maximum velocity response. As

shown in all cases, the maximum velocity responses are smaller for the collocated sensor/actuator design compare to the non-collocated sensor/actuator design. See Table 5.7. In case 1, the optimally located non-collocated sensor/actuator design's relative error in estimating the true state response is smaller than the optimally located collocated sensor/actuator design's. In other cases, the relative error in estimation deflection response of the non-collocated sensor/actuator design is not always the smallest compare to other sensor/actuator locations. See Table 5.8 for the listings of the relative error values in estimations of deflection and velocity responses. See Figures 5.5, 5.7 and 5.9 for comparisons of the non-collocated sensor/actuator and collocated sensor/actuator controller performances.

The actuator location seems to dominate the performance index values, especially in case 1. In the non-collocated sensor/actuator design, as shown in the contour plots of $J^*(l, r)$ in Figures 5.4, 5.6, and 5.8, the graph $J^*(l, r)$ resembles a steeper concave up in the actuator r dimension and almost constant in the sensor l dimension. Moreover, the performances of a randomly located non-collocated sensor/actuator controller with its actuator located at the optimal actuator location, r^*, result in smaller performance index and controlled responses than a non-optimal collocated sensor/actuator controller located at the optimal non-collocated sensor location l^*. As shown in Figure 5.10, the velocity responses of the non-collocated sensor/actuator controller at (l, r^*), l being a randomly selected sensor location in each case, resembles a similar velocity responses at the non-collocated sensor/actuator optimal location in case 1. Its estimated velocity is slightly poorer. As shown in Figure 5.11, the velocity responses of the collocated sensor/actuator controller at l^* are larger in maximum amplitudes (poorer control performance) but with a better estimation on velocity.

When the optimal actuator location is fixed at the optimal non-collocated sensor/actuator actuator location r^*, in case 2 and 3 (the scale of the location optimization cost functional range is relatively smaller), the controlled responses at different sensor locations yields worse, but small differences, responses than the optimal located non-collocated sensor/actuator at (l^*, r^*). In case 1, (the scale of the location optimization cost functional range is relatively larger), the controlled responses at different sensor locations yield almost identical responses to the optimal located non-collocated sensor/actuator at (l^*, r^*). Note that the sensor noise is set to be relatively large in this thesis. See Figure 5.12 and Figure 5.13.

The sensor locations affect the estimation of the true responses, but do not significantly affect the control performances. Collocated design at the optimal sensor locations,

l^*, tend to have the smallest relative errors in estimations. Non-collocated design with randomly located sensors tends to have the largest relative errors in estimations. See Table 5.8.

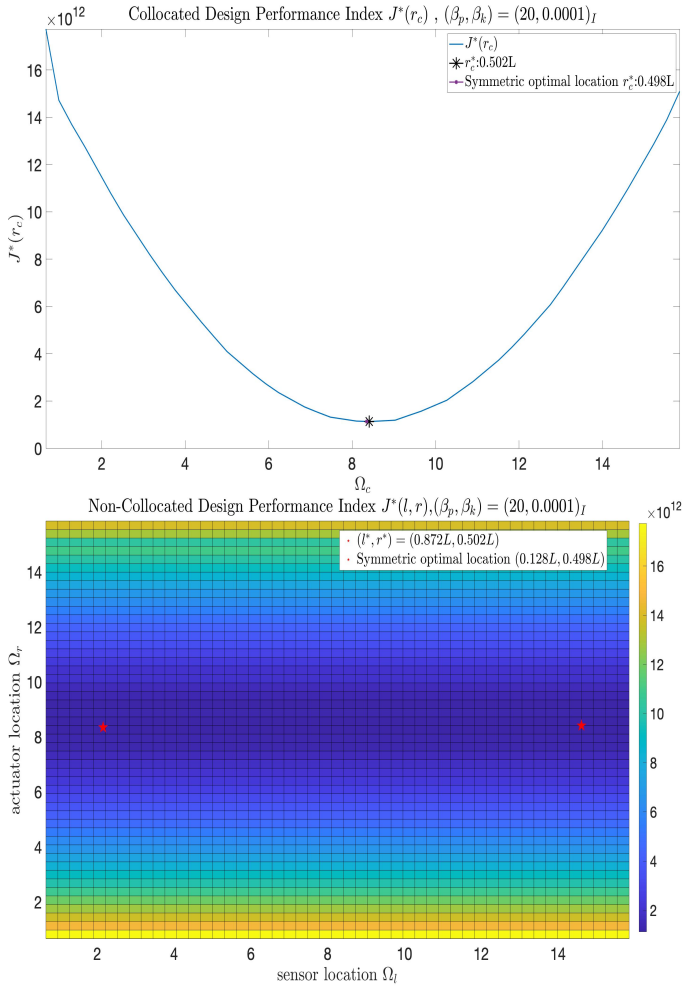

Figure 5.4: Case 1: $Q_0 = (20, 0.0001)_I$.
Collocated performance index vs. Ω_c, $J^*(r_c^*) = J^*(0.502L) = 1.1312 \times 10^{12}$ (top).
Non-collocated performance index vs. Ω_s, $J^*(l^*, r^*) = J^*(0.872L, 0.502L) = 1.1311 \times 10^{12}$ (bottom).

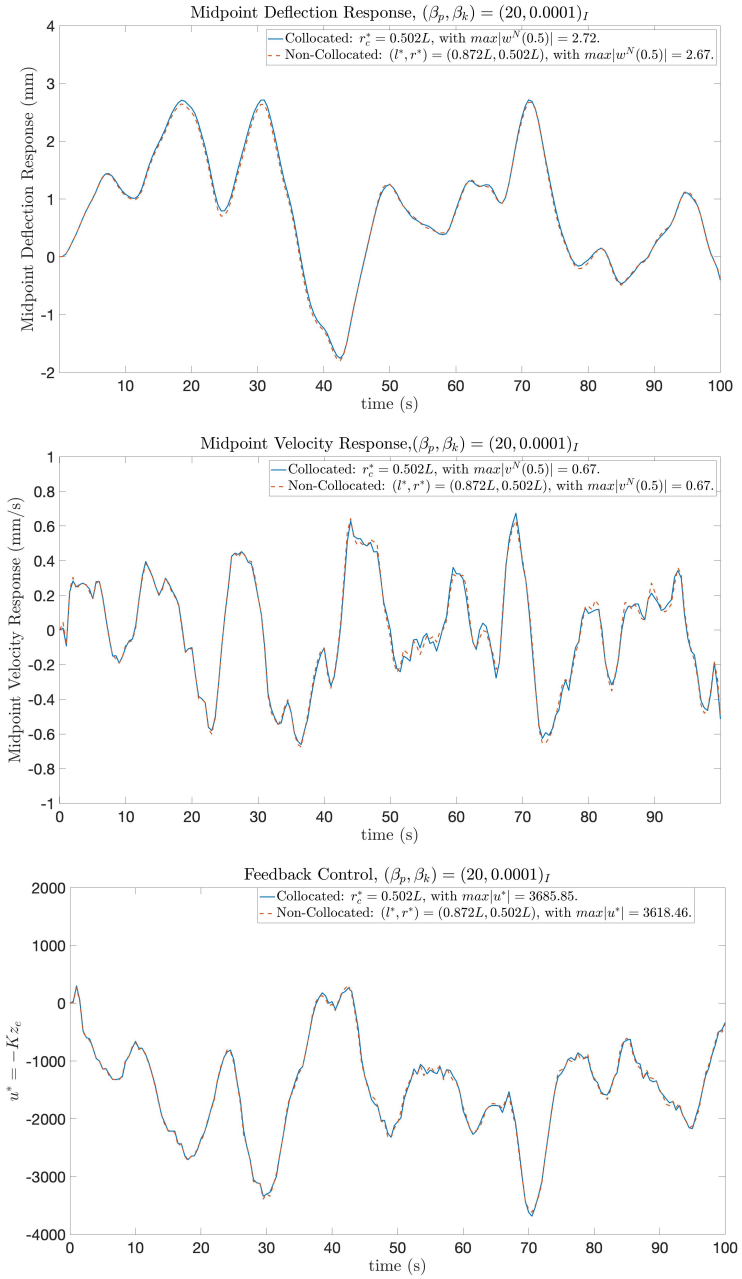

Figure 5.5: Case 1: $Q_0 = (20, 0.0001)_I$.
Compare performances of non-collocated sensor/actuator and collocated sensor/actuator at their optimal locations. Compare deflection responses (top). Compare velocity responses (middle). Compare feedback control (bottom).

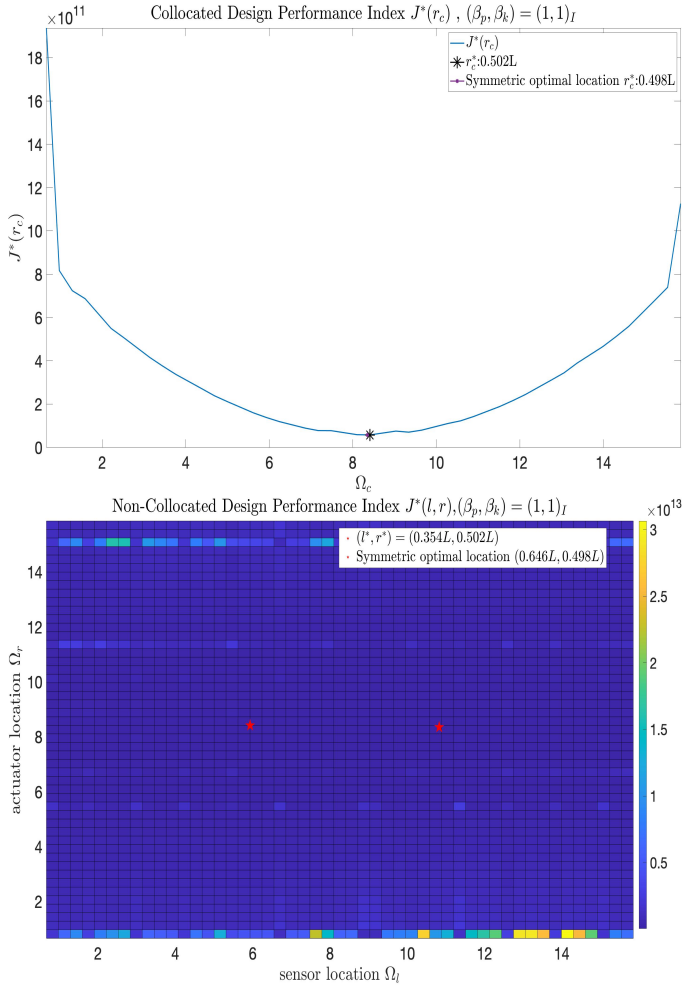

Figure 5.6: Case 2 $Q_0 = (1,1)_I$.
Collocated performance index vs. Ω_c,$J^*(r_c^*) = J^*(0.502L) = 5.73 \times 10^{10}$ (top).
Non-collocated performance index vs. Ω_s, $J^*(l^*, r^*) = J^*(0.354L, 0.502L) = 5.67 \times 10^{10}$ (bottom).

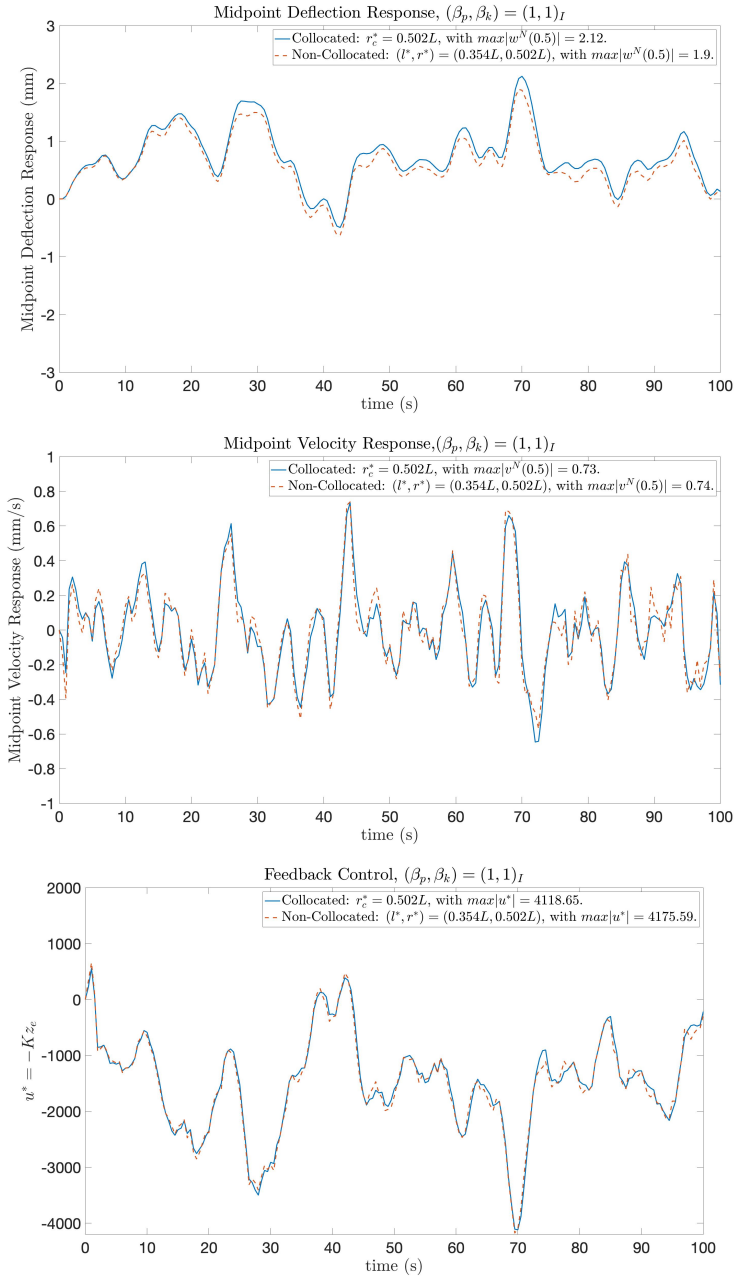

Figure 5.7: Case 2: $Q_0 = (1,1)_I$.
Compare performances of non-collocated sensor/actuator and collocated sensor/actuator at their optimal locations. Compare deflection responses (top). Compare velocity responses (middle). Compare feedback control (bottom).

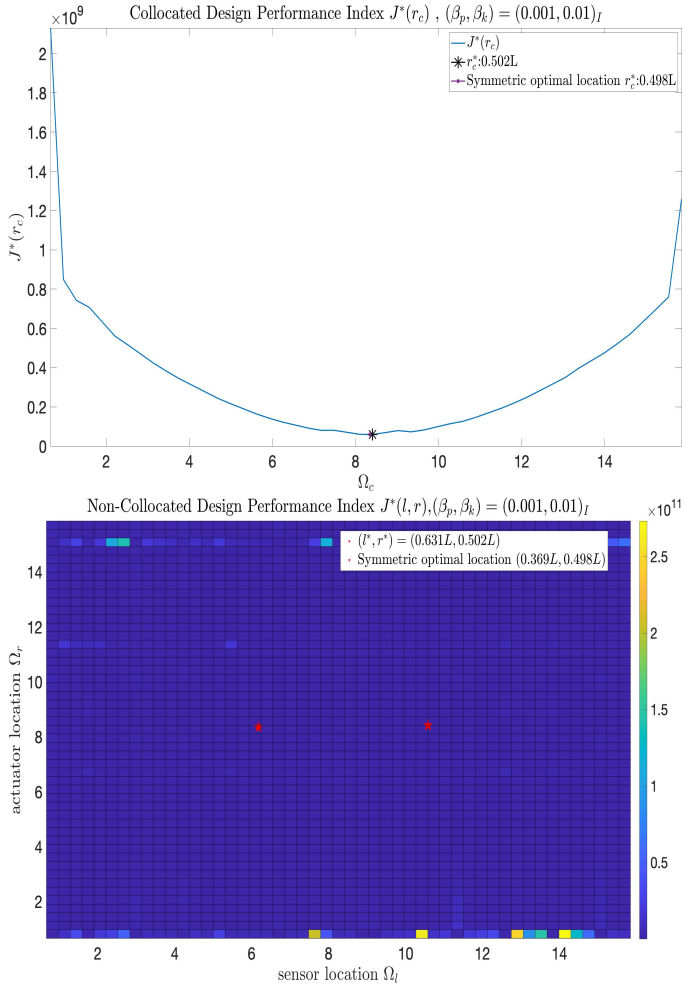

Figure 5.8: Case 3: $Q_0 = (0.001, 0.01)_I$.
Collocated performance index vs. Ω_c, $J^*(r_c^*) = J^*(0.502L) = 5.79 \times 10^7$ (top).
Non-collocated performance index vs. Ω_s, $J^*(l^*, r^*) = J^*(0.631L, 0.502L) = 5.79 \times 10^7$ (bottom).

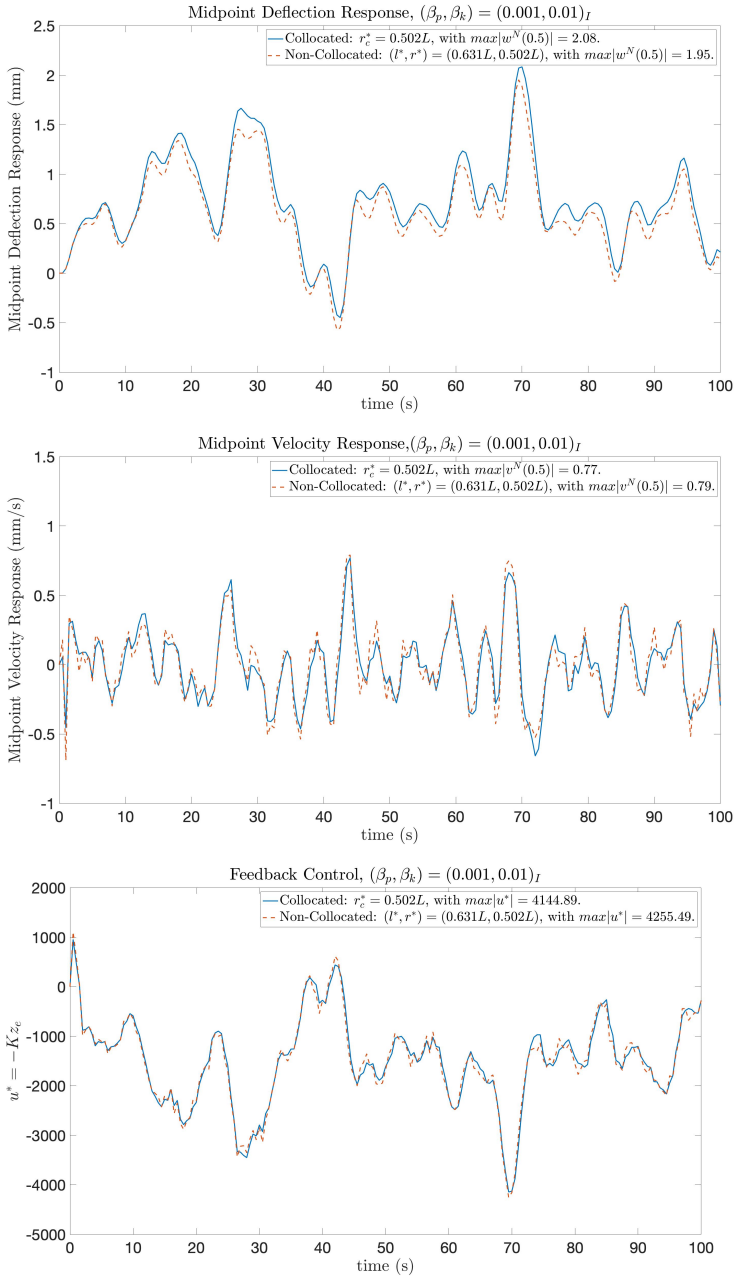

Figure 5.9: Case 3: $Q_0 = (0.001, 0.01)_I$.
Compare performances of non-collocated sensor/actuator and collocated sensor/actuator at their optimal locations. Compare deflection responses (top). Compare velocity responses (middle). Compare feedback control (bottom).

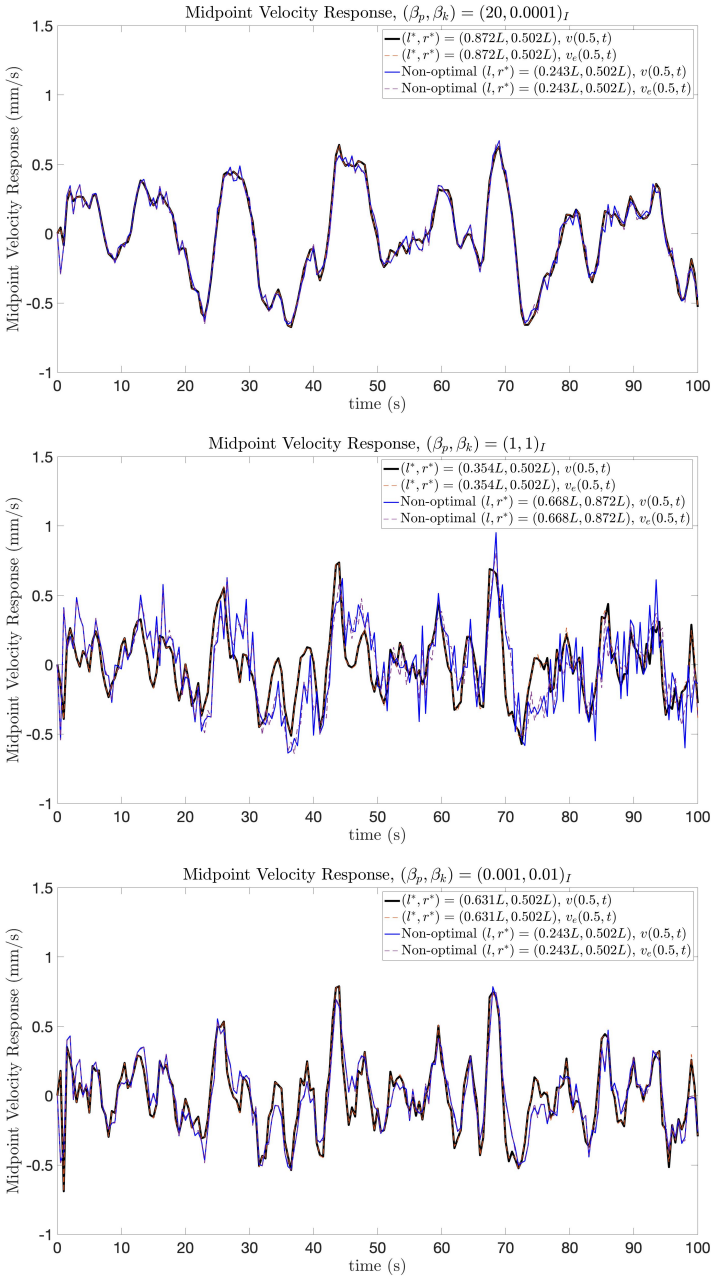

Figure 5.10: Compare velocity estimations of the optimally located non-collocated sensor/actuator design to the non-collocated sensor/actuator design at a random sensor and optimal actuator location (l, r^*). Case 1, $(l, r^*) = (0.243L, r^*)$ (top). Case 2, $(l, r^*) = (0.668, r^*)$ (middle). Case 3, $(l, r^*) = (0.243L, r^*)$ (bottom).

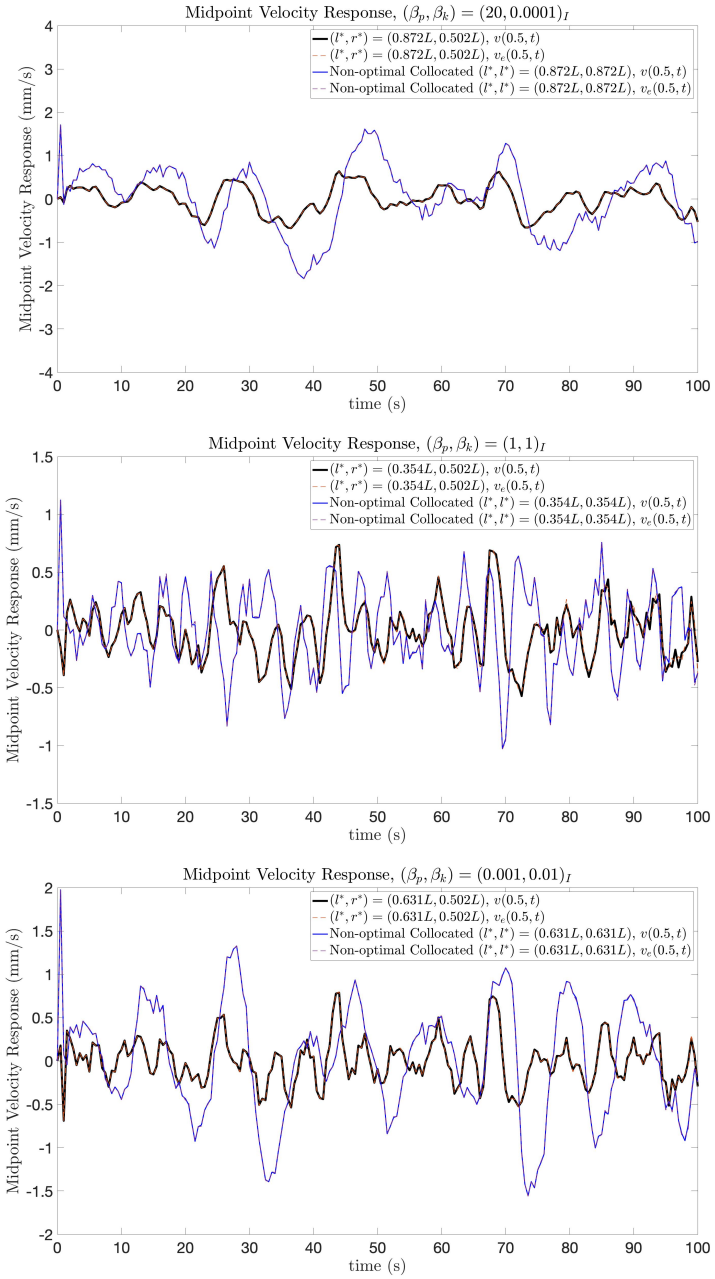

Figure 5.11: Compare velocity estimations of the optimally located non-collocated sensor/actuator design to the collocated design at the optimal non-collocated sensor location l^*. Case 1 (top). Case 2 (middle). Case 3 (bottom).

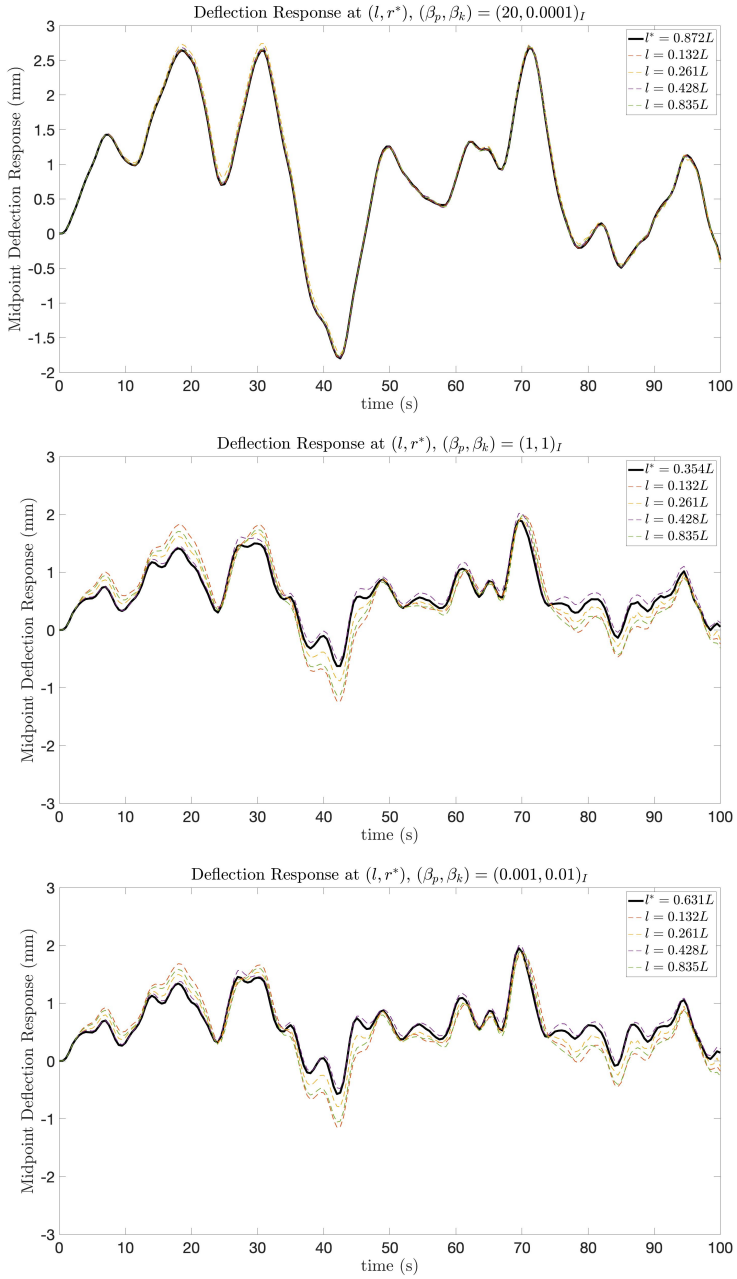

Figure 5.12: Compare deflection responses at fixed optimal actuator location r^*, with varying sensor location l. Case 1 (top). Case 2 (middle).Case 3 (bottom).

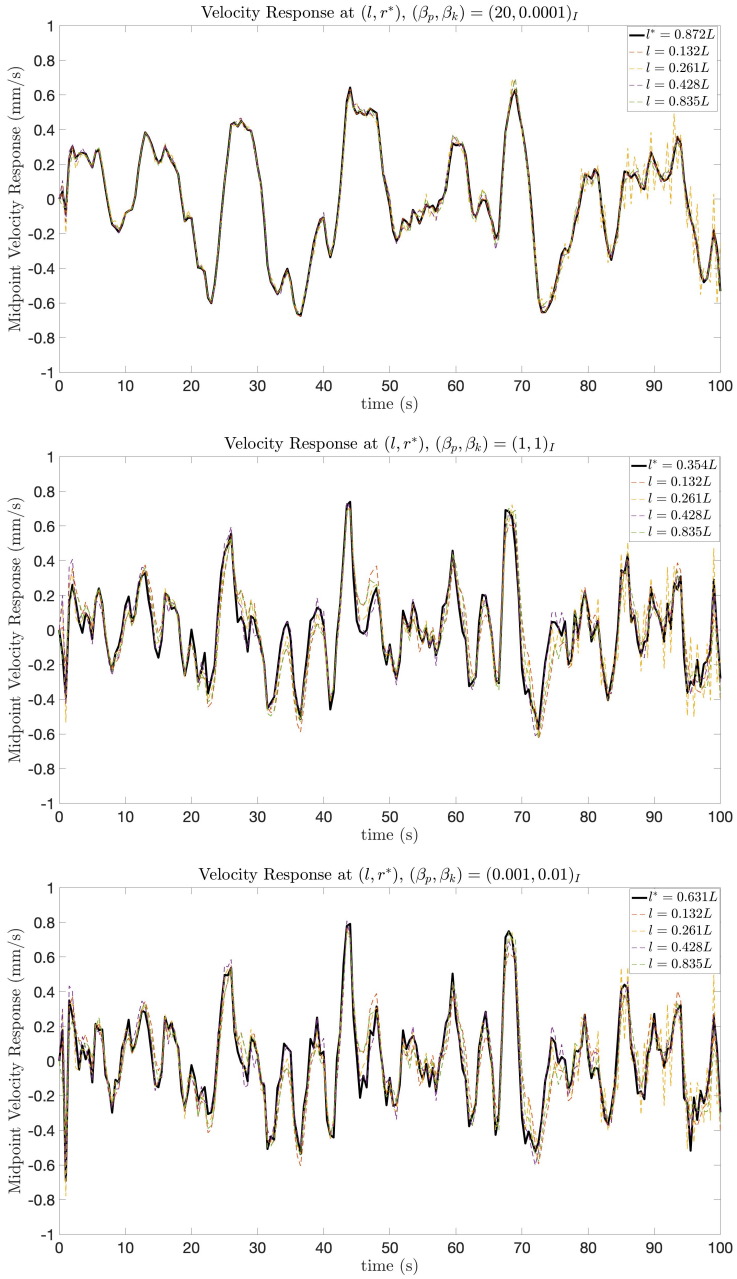

Figure 5.13: Compare velocity responses at fixed optimal actuator location r^*, with varying sensor location l. Case 1 (top). Case 2 (middle). Case 3 (bottom).

Chapter 6

Conclusion and Future Extensions

In this thesis, the optimal locations of the separated and the collocated sensor/actuator design for a lightweight aluminum pedestrian bridge are studied. The controlled responses at the optimal locations of the two controller designs are compared.

A simple beam structure and the realistic bridge system in this thesis are modelled based on the Euler-Bernoulli beam theory. Two numerical approximation methods are used.

The LQ objective-driven controller for the approximated finite-dimensional system is reviewed. The sensor/actuator location-parameterized LQ controller and the separated and collocated location optimization problems are defined. An explanation of developing the state energy weight mapping from the original infinite-dimensional functional space to the approximated finite-dimensional functional space is included in this thesis.

In the preliminary problem, the modal approximation is used to approximate this simplified model. The LQG controller is reviewed and applied. The numerical implementation of stochastic disturbances is presented. The numerical complications on inverting large matrix and simulating ill-condition matrix are discussed and provided with solutions. Simulation results are consistent with [1] that weighting on the velocity state effectively improves the controlled response, and are consistent with [36] that increasing on the state weight moves the optimal actuator locations from the center. Depending on the state weights and disturbance distributions, the collocated sensor/actuator design at the optimal locations

can achieve the same control performance as that of the non-collocated design at the optimal locations.

In the bridge model, Hermite basis FEM approximation is used to approximate a more realistic pedestrian bridge model. The $\mathbb{H}_2$ controller is reviewed and applied. To consider more realistic situations, the actuator device dynamics and its noise, the pedestrian load referencing from [13], and a low pass filter are included in the model. Interestingly, this augmented model resulted in that the optimal estimator depends on both of the sensor and actuator locations.

The main simulation results show that, although the optimally located non-collocated sensor/actuator design yields the smallest performance index, it is only relatively smaller to the optimally located collocated sensor/actuator performance index by at most 2%. The controlled responses are almost identical. The optimally located non-collocated sensor/actuator design yields a relatively smaller $\mathcal{L}_2$-norm and maximum amplitude of the deflection response by at most 12%, but a relatively larger $\mathcal{L}_2$-norm and maximum amplitude of the velocity response by at most 3.33%. In case 1 (the scale of the location optimization cost functional range is relatively large), the difference in the two optimally located designs' optimal performance index values vanishes, and the differences in their performances diminish. The results suggest that the physically more practical collocated sensor/actuator design can achieve performances as excellently as the ideally more optimal non-collocated sensor/actuator design at their corresponding optimal locations.

Future extensions can be done by investigating the optimal locations of the sensor/actuator by considering more realistic factors to the structural model and control design. The structure can be extended to a more complicated bridge model such as the Timoshenko beam model with the shear deformation or a higher dimensional bridge model with the deformations in the horizontal direction. Non-simply supported structures can be considered to study the differences between the two controller designs when symmetry of the structure is absent. Realistically, disturbances are unpredictable. Therefore, by using the $\mathbb{H}_\infty$-controller design, the control design can be extended to the robustness of the system against unknown disturbances.

References

[1] K.K. Ang, S.Y. Wang, and S.T. Quek. Weighted energy linear-quadratic regulator vibration control of piezoelectric composite plates. *Smart Materials and Structures*, vol. 11(no. 1):pp. 98–106, Feb. 2002.

[2] A. Bensoussan. *Estimation and Control of Dynamical Systems*. Springer International Publishing AG, 2018.

[3] C. Bergeling, K.A. Morris, and A. Rantzer. Closed-form $\mathbb{H}_\infty$ optimal control for a class of infinite-dimensional systems. *Automatica (Oxford)*, vol. 117:pp. 108916, July 2020.

[4] A.E. Bryson and Y. Ho. *Applied Optimal Control: Optimization, Estimation, and Control*. Rev. printing, Hemisphere Pub. Corp, 1975.

[5] C. Caprani and E. Ahmadi. Formulation of human–structure interaction system models for vertical vibration. *Journal of Sound and Vibration*, vol. 377:pp. 346–367, 2016.

[6] K.K. Chen and C.W. Rowley. $\mathbb{H}_2$ optimal actuator and sensor placement in the linearised complex ginzburg-landau system. *Journal of Fluid Mechanics*, vol. 681:pp. 241–60, Aug. 2011.

[7] J.P. Corriou. *Coulson and Richardson's Chemical Engineering, Fourth Edition, Chapter 10 - Optimal Control*. Elsevier Ltd, 2017.

[8] R.F. Curtain and A. Ichikawa. The separation principle for stochastic evolution equations. *SIAM Journal on Control and Optimization*, vol. 15(no. 3):pp. 367–83, May 1977.

[9] N. Darivandi, K.A. Morris, and A. Khajepour. An algorithm for LQ optimal actuator location. *Smart Materials and Structures*, vol.22(no. 3):p. 35001, 2013.

[10] M.A. Demetriou. A numerical algorithm for the optimal placement of actuators and sensors for flexible structures. *Proceedings of the 2000 American Control Conference. ACC (IEEE Cat. No.00CH36334).*, vol. 4:pp. 2290–2294, 2000.

[11] M.A. Demetriou. Integrated actuator-sensor placement and hybrid controller design of flexible structures under worst case spatiotemporal disturbance variations. *Journal of Intelligent Material Systems and Structures*, vol. 15(no. 12):pp. 901–21, Dec. 2004.

[12] M.A. Demetriou and N. Kazantzis. A new integrated output feedback controller synthesis and collocated actuator/sensor scheduling framework for distributed parameter processes. *Computers Chemical Engineering*, vol. 29(no. 4):pp. 867–76, 2005.

[13] P. Dey, A. Sychterz, S. Narasimhan, and S. Walbridge. Performance of pedestrian-load models through experimental studies on lightweight aluminum bridges. *Journal of Bridge Engineering*, vol. 21(no. 8), 2016.

[14] F. Fahroo and M.A. Demetriou. Optimal actuator/sensor location for active noise regulator and tracking control problems. *Journal of Computational and Applied Mathematics*, vol. 114(no. 1):pp. 137–58, 2000.

[15] J. Fish and T. Belytschko. *First Course in Finite Elements*. Chichester: Wiley, 2007.

[16] K. Goorts and S. Narasimhan. Adaptive model predictive control for deployable control systems with constraints. *Journal of Structural Engineering*, vol. 145(no. 10):p. 4019110, 2019.

[17] M. Güney and E. Eşkinat. Optimal actuator and sensor placement in flexible structures using closed-loop criteria. *Journal of Sound and Vibration*, vol. 312(no. 1):pp. 210–33, 2008.

[18] V. Gupta, M. Sharma, and N. Thakur. Optimization criteria for optimal placement of piezoelectric sensors and actuators on a smart structure: A technical review. *Journal of Intelligent Material Systems and Structures*, vol. 21(no. 12):pp. 1227–43, Aug. 2010.

[19] A. Hać and L. Liu. Sensor and actuator location in motion control of flexible structures. *Journal of Sound and Vibration*, vol. 167(no. 2):pp. 239–61, 1993.

[20] S.M. Hasheminejad and A. Oveisi. Active vibration control of an arbitrary thick smart cylindrical panel with optimally placed piezoelectric sensor/actuator pairs. *International Journal of Mechanics and Materials in Design*, vol. 12(no. 1):pp. 1–16, 2015.

[21] E. Hendricks, O. Jannerup, and P.H. Sorensen. *Linear Systems Control: Deterministic and Stochastic Methods.* Linear Systems Control, 1. Aufl., Springer-Verlag, 2008.

[22] C.H. Houpis and C.T. Constantinides. Correlation between conventional control figures of merit and the Q matrix of the quadratic cost function: third-order plant. *International Journal of Control*, vol. 16(no. 4):pp. 695–704, Oct. 1972.

[23] A. Ichikawa and E.P. Ryan. Sensor and controller location problems for distributed parameter systems. *Automatica*, vol. 15(no. 3):pp. 347–352, 1979.

[24] B. Jacob and K.A. Morris. Second-order systems with acceleration measurements. *IEEE Transactions on Automatic Control*, vol. 57(no. 3):pp. 690–700, 2016.

[25] W. Kang and L. Xu. Optimal placement of mobile sensors for data assimilations. *Tellus. Series A, Dynamic Meteorology and Oceanography*, vol. 64(no. 1):pp. 17133–12, Dec. 2012.

[26] D. Kasinathan and K.A. Morris. $\mathbb{H}_\infty$-optimal actuator location. *IEEE Transactions on Automatic Control*, vol. 58(no. 10):pp. 2522–35, Oct. 2013.

[27] B. Ko, B.H. Tongue, and A. Packard. A method for determining the optimal location of a distributed sensor/actuator. *Shock and Vibration*, vol. 1(no. 4):pp. 357–74,, Jan. 1994.

[28] P.R. Kumar and P.P. Varaiya. *Stochastic Systems: Estimation, Identification, and Adaptive Control.* Prentice Hall., 1986.

[29] F. Liu, P. Li, Z. Lei, and Y. Song. Linear-quadratic optimal sampled data control of linear systems with unknown switched modes and stochastic disturbances: Linear-quadratic optimal sampled data control. *Optimal Control Applications Methods*, vol. 37(no. 5):pp. 1085–100, Sept. 2016.

[30] W. Liu, Z. Hou, and M.A. Demetriou. A computational scheme for the optimal sensor/actuator placement of flexible structures using spatial $\mathbb{H}_2$ measures. *Mechanical Systems and Signal Processing*, vol. 20(no. 4):pp. 881–95, 2006.

[31] S.O.R. Moheimani and T. Ryall. Considerations on placement of piezoceramic actuators that are used in structural vibration control. *Proceedings of the 38th IEEE Conference on Decision and Control (Cat. No.99CH36304)*, vol. 2:pp. 1118–1123, 1999.

[32] K.A. Morris. *Controller Design for Distributed Parameter Systems.* Springer International Publishing AG, 2020.

[33] K.A. Morris. Optimal output estimation for infinite-dimensional systems with disturbances. *Systems Control Letters*, vol. 146:p. 104803, 2020.

[34] K.A. Morris. Linear-quadratic optimal actuator location. *IEEE Transactions On Automatic Control*, vol. 56(no. 1):pp. 113–124, Jan. 2011.

[35] K.A. Morris, M.A. Demetriou, and S.D. Yang. Using $\mathbb{H}_2$-control performance metrics for the optimal actuator location of distributed parameter systems. *IEEE Transactions on Automatic Control,*, vol. 60(no. 2):pp. 450–462, Feb. 2015.

[36] K.A. Morris and S.D. Yang. Comparison of actuator placement criteria for control of structures. *Journal of Sound and Vibration*, vol. 353:pp. 1–18, Sept. 2015.

[37] U. Munz, M. Pfister, and P. Wolfrum. Sensor and actuator placement for linear systems based on $\mathbb{H}_2$ and $\mathbb{H}_\infty$ optimization. *IEEE Transactions on Automatic Control*, vol. 59(no. 11):pp. 2984–89, Nov. 2014.

[38] H. Ohta, P.N. Nikiforuk, and M. Kakinuma. Use of negative weights in linear-quadratic regulator synthesis. *Journal of Guidance, Control, and Dynamics*, vol. 14(no. 4):pp. 791–96, July 1991.

[39] E. Ostertag. *Mono-and Multivariable Control and Estimation: Linear, Quadratic and LMI Methods.Vol. 2.* Springer, 2011.

[40] F. Palacios-Quiñonero, J. Rubió-Massegú, J. Rossell, and J. Rodellar. Design of distributed multi-actuator systems with incomplete state information for vibration control of large structures. *Designs*, vol. 2(no. 1):p. 6, Feb. 2018.

[41] R. Potami. *Optimal sensor/actuator placement and switching schemes for control of flexible structures, PH.D thesis,*. PhD thesis, Worcester Polytechnic Institute, Worcester, 2008.

[42] B. Prakash, M.Y. Yasin, A.H. Khan, M. Asjad, and Z.A. Khan. Optimal location and geometry of sensors and actuators for active vibration control of smart composite beams. *Australian Journal of Mechanical Engineering*, pages pp. 1–19,, June 2020.

[43] B. Pridham, T. Normile, C. Kronenwetter, P. Reynolds, and E. Hudson. Control of traffic-induced ground vibrations in a residential structure. In *Pakzad S. (eds) Dynamics of Civil Structures*, volume vol.2 of *Conference Proceedings of the Society for Experimental Mechanics Series*. Springer, 2021.

[44] K. Ramesh-Kumar and S. Narayanan. The optimal location of piezoelectric actuators and sensors for vibration control of plates. *Smart Materials and Structures*, vol. 16(no. 6):pp. 2680–91, Dec. 2007.

[45] K. Ramesh-Kumar and S. Narayanan. Active vibration control of beams with optimal placement of piezoelectric sensor/actuator pairs. *Smart Materials and Structures*, vol. 17(no. 5):p. 055008, Oct. 2008.

[46] T. Roy and D. Chakraborty. Optimal vibration control of smart fiber reinforced composite shell structures using improved genetic algorithm. *Journal of Sound and Vibration*, vol. 319(no. 1):pp. 15–40, 2009.

[47] H.R. Shaker and M. Tahavori. Optimal sensor and actuator location for unstable systems. *Journal of Vibration and Control*, vol. 19(no. 12):pp. 1915–20, Sept. 2013.

[48] V.A. Ugrinovskii and I.R. Petersen. Minimax LQG control of stochastic partially observed uncertain systems. *SIAM Journal on Control and Optimization*, vol. 40(no. 2):pp. 1189–226, 2002.

[49] B. Yassin, A. Lahcen, and E.M. Zeriab. Hybrid optimization procedure applied to optimal location finding for piezoelectric actuators and sensors for active vibration control. *Applied Mathematical Modelling*, vol. 62:pp. 701–16, Oct. 2018.

[50] M. Zhang and K.A. Morris. Sensor choice for minimum error variance estimation. *IEEE Transactions on Automatic Control*, vol. 63(no. 2):pp. 315–30, Feb. 2018.

[51] K. Zhou and J.C. Doyle. *Essentials of Robust Control*. Upper Saddle River, N.J: Prentice Hall, 1998.

[52] N.D. Zorić, A.M. Simonović, Z.S. Mitrović, and S.N. Stupar. Optimal vibration control of smart composite beams with optimal size and location of piezoelectric sensing and actuation. *Journal of Intelligent Material Systems and Structures*, vol. 24(no. 4):pp. 499–526, Mar. 2013.